



1 **Extended Bloch-McConnell equations for mechanistic**
2 **analysis of hyperpolarized ^{13}C magnetic resonance**
3 **experiments on enzyme systems**

4 Thomas R. Eykyn¹, Stuart J. Elliott^{2,4} and Philip W. Kuchel³

5 ¹ School of Biomedical Engineering and Imaging Sciences, King's College London, St Thomas' Hospital,
6 London SE1 7EH, United Kingdom

7 ² Centre de Résonance Magnétique Nucléaire à Très Hauts Champs - FRE 2034 Université de Lyon / CNRS /
8 Université Claude Bernard Lyon 1 / ENS de Lyon, 5 Rue de la Doua, 69100 Villeurbanne, France

9 ³ School of Life and Environmental Sciences, University of Sydney, NSW 2006, Australia

10 ⁴ Current address: Department of Chemistry, University of Liverpool, Liverpool L69 7ZD, United Kingdom

11 *Correspondence to:* Thomas R. Eykyn (thomas.eykyn@kcl.ac.uk)

12 This article is dedicated to Geoffrey Bodenhausen on the occasion of his 70th Birthday.

13 **Abstract.** We describe an approach to formulating the kinetic master equations of the time evolution of NMR
14 signals in reacting (bio)chemical systems. Special focus is given to studies that employ signal enhancement
15 (hyperpolarization) methods such as dissolution dynamic nuclear polarization (dDNP) and involving nuclear spin-
16 bearing solutes that undergo reactions mediated by enzymes and membrane transport proteins. We extend the
17 work given in a recent presentation on this topic to now include enzymes with two or more substrates and various
18 enzyme reaction mechanisms as classified by Cleland. Using this approach, we can address some pressing
19 questions in the field from a theoretical standpoint. For example, why does binding of a hyperpolarized substrate
20 to an enzyme *not* cause an appreciable loss of the signal from the substrate or product? Why does the concentration
21 of an unlabelled pool of substrate, for example ^{12}C lactate, cause an increase in the rate of exchange of the ^{13}C
22 labelled pool? To what extent is the equilibrium position of the reaction perturbed during administration of the
23 substrate? The formalism gives a full mechanistic understanding of the time courses derived and is of relevance
24 to ongoing clinical trials using these techniques.

25

26 **1 Introduction**

27 Nuclear magnetic resonance (NMR) spectroscopy and imaging (MRI) are widely employed techniques with far-
28 reaching applications in physics, chemistry, medicine and the life sciences. NMR and MRI provide a wealth of
29 information from structure elucidation, protein dynamics and metabolic profiling through to disease diagnostics
30 in oncology, cardiology and neurology among others. The technique's low sensitivity is one of the primary
31 concerns in the magnetic resonance community and is often a limiting factor in experiments from solid-state NMR
32 to medical imaging. Recent work has shown that the sensitivity of NMR experiments can be improved by using
33 non-equilibrium hyperpolarization techniques such as dissolution dynamic nuclear polarization (dDNP) to boost
34 signal intensities by many orders of magnitude (Ardenkjaer-Larsen et al., 2003). Such techniques have led to new
35 applications (Golman et al., 2003; Golman et al., 2006; Keshari and Wilson, 2014) and necessitated the
36 development of acquisition strategies to exploit the hyperpolarized magnetization in a time efficient manner (Yen
37 et al., 2009); as well as new tools for signal processing and image reconstruction (Hu et al., 2010). A challenge



38 with the interpretation of these recordings is that, unlike radiotracers, hyperpolarized MR is a non-tracer technique
39 requiring the injection of physiological or even supra-physiological concentrations of substrate.

40 To date there have been many mathematical methods devised for analyzing the kinetic time courses in
41 dDNP NMR studies (Zierhut et al., 2010; Hill et al., 2013b; Pagès and Kuchel, 2015; Daniels et al., 2016).
42 However, until recently there has been little consensus on the best methods for analyzing and then interpreting
43 reaction kinetics measured therein. A theoretical framework has only recently appeared to fully elucidate the
44 underlying mechanisms (Kuchel and Shishmarev, 2020). One challenge is that the widely used Bloch-McConnell
45 equations describe the exchange of magnetization of only the MR active nuclei while the reaction kinetics are
46 subject to a plethora of molecular interactions in a (bio)chemical milieu. Furthermore, in a typical hyperpolarized
47 MR experiment the initial injection of a non-tracer concentration of substrate causes the reaction system to be
48 perturbed from its equilibrium state, or quasi-steady state, and therefore the concentrations of the reactants are
49 time dependent. In this regard, challenges relate to the description of non-linear kinetics, for example second order
50 reactions, and the involvement of un-observable (non-labelled) metabolites to the overall kinetics, *e.g.*, enzyme
51 cofactors, co-substrates and natural abundance ^{12}C -containing metabolites (Hill et al., 2013a); as well as explicit
52 descriptions of enzyme mechanisms *e.g.*, sequential ordered, sequential random, double displacement (ping-pong)
53 reactions, and allosteric interactions that occur on an enzyme far from its active site. Enzyme activity is also
54 influenced by inhibitors that can be competitive, non-competitive, or uncompetitive (Cook and Cleland, 2007;
55 Cleland, 1967). Mathematical models of enzyme systems should agree with standard descriptions of (bio)chemical
56 kinetics while remaining capable of describing the time evolution of magnetization that is described by the Bloch-
57 McConnell equations (McConnell, 1958).

58 Here we address these issues in a stepwise manner, by developing a mechanistic approach that combines
59 the MR interactions with the chemical and/or enzyme mediated reactions described by the Bloch-McConnell
60 equations. These equations are grounded in the concept of conservation of mass of the hyperpolarized signal plus
61 its non-hyperpolarized counterpart and the various products; this was recently highlighted (Kuchel and
62 Shishmarev, 2020) where the MR visible signal decays to produce an MR invisible one such that the sum is
63 constant and proportional to the total solute concentration.

64

65 **1.1 Basic concepts – sensitivity**

66 We begin addressing the problem by defining the signal-to-noise ratio (SNR) in MR. In its most basic form,
67 sensitivity is described by the ratio of the signal amplitude divided by the root mean square of the amplitude of
68 the noise. When a signal $S(t)$ is detected in the NMR receiver coil that surrounds the sample, the magnitude of
69 the induced current is a function of: (i) the perturbation of nuclear spin populations from thermal equilibrium
70 $S_{sample}(t)$; plus (ii) a random contribution from the noise in the electronic circuitry $S_{electronics}(t)$. Hence:

71

$$S(t) = S_{sample}(t) + S_{electronics}(t) \quad (1)$$

72

73 The current induced in the coil is time-dependent and proportional to the magnetization that precesses in the x,y -
74 plane. In other words, the signal $S(t)$ is recorded until decoherence renders $S_{sample}(t)$ undetectable against the



75 noise, $S_{electronics}(t)$. The latter is mainly attributed to the radiofrequency (RF) circuitry in the probe head and the
76 preamplifier(s) (e.g., Johnson noise (Johnson, 1928)) of the spectrometer. If the NMR signal (free induction decay;
77 FID) that is detected in a subsequent experiment is indistinguishable from the first, and the two are added together,
78 then the signal amplitude (peak area) will scale linearly with the number of added FIDs, N . The noise associated
79 with each experiment is random, and assuming its source remains fixed over time, i.e., stationary noise, then the
80 amplitude scales with the square root of the number of FIDs, $N^{1/2}$. Hence signal summation enhances the SNR
81 of an NMR experiment in proportion to the square root of the number of FIDs. In other words, to achieve an
82 enhancement by a factor ξ requires an increase in experiment duration of ξ^2 . Therefore, unavoidably, FID
83 summation is a slow process and experiments can sometimes take days or weeks to achieve a sufficient SNR from
84 a sample of a low sensitivity nuclide or one with a long relaxation time. The amount of attainable signal averaging
85 is constrained when monitoring dynamic processes by NMR spectroscopy; and an inherently good SNR is
86 required from the outset for a time course experiment.

87

88 1.2 Thermal effects

89 The usual way to proceed when calculating the NMR response of a spin system to RF pulse sequences
90 is to solve the ordinary quantum mechanical master equation that describes the evolution of the spin density
91 operator (Hore et al., 2015). This is the Liouville-von Neumann equation, that has been extended to include non-
92 coherent interactions (predominantly relaxation phenomena) (Ernst et al., 1987):

93

$$\frac{d}{dt}\rho = -i\hat{H}\rho - \hat{T}(\rho - \rho_0) \quad , \quad (2)$$

94

95 where \hat{H} is the commutation superoperator of the coherent Hamiltonian H given by $\hat{H}\rho = [H, \rho]$, which contains
96 information on all spin-spin and field-spin interactions; while \hat{T} is the relaxation superoperator that describes all
97 longitudinal (T_1) and transverse (T_2) relaxation processes, as well as any cross-relaxation or cross-correlation
98 interactions. Note, that in the interests of reducing clutter in equations (for which the operator context should be
99 clear) hereafter we have omitted carets denoting operators and only used them to denote superoperators.

100 Our aim here is to describe the kinetics of exchange between different solutes that contain hyperpolarized
101 nuclei e.g., $A \leftrightarrow B$, in which the relaxation times are constant. In this quest, the first simplifying assumption that
102 is worth exploring is that all intermolecular interactions, notably, scalar coupling, dipolar coupling, cross-
103 relaxation and cross-correlation between species A and B can be ignored. This applies to non-interacting solute
104 molecules in solution in which motional averaging occurs; and we focus on thermal effects on the evolution of
105 the FID.

106 The so-called Zeeman polarization term describes the sensitivity of $S_{sample}(t)$ in Eq. (1) to temperature
107 and magnetic field in an NMR experiment. Magnetic polarization is described by the equilibrium density operator
108 ρ_0 that specifies the probability distribution of states. Zeeman polarization corresponds to the magnitude of
109 normalized longitudinal spin order I_z that is contained in ρ_0 . Specifically, for an ensemble of spin- $1/2$ nuclei this
110 is given by (Ernst et al., 1987):

111



$$\rho_0 = \frac{\exp(-\hbar H_0/kT)}{\text{Tr}\{\exp(-\hbar H_0/kT)\}} \quad (3)$$

112

113 where k is the Boltzmann constant and T is the temperature (Kelvin). The Zeeman Hamiltonian H_0 describes the
114 interaction of the spins with the static magnetic field of magnitude B_0 , given by $H_0 = \omega_0 I_z$, where ω_0 is the
115 Larmor frequency (rad s⁻¹). In the basis of the two eigenstates $|\alpha\rangle$ (“spin-up”) and $|\beta\rangle$ (“spin-down”), the
116 equilibrium density operator is written in matrix form as:

117

$$\rho_0 = \frac{1}{Z} \begin{bmatrix} \exp(\hbar\omega_0/2kT) & 0 \\ 0 & \exp(-\hbar\omega_0/2kT) \end{bmatrix} \quad (4)$$

118

119 where Z is the partition function, given by $Z = \sum_{i=1}^M \exp(-\varepsilon_i/kT)$, and M is the number of states ($M = 2$ for an I
120 = $\frac{1}{2}$ nucleus). In the case of a spin- $\frac{1}{2}$ system, the partition function is the sum of the populations $Z =$
121 $\exp(\hbar\omega_0/2kT) + \exp(-\hbar\omega_0/2kT) \approx 2$ when ε_i is very small, as is typically the case at thermal equilibrium
122 in NMR systems. The Zeeman polarization is proportional to the projection of the spin density operator onto the
123 angular momentum operator. In other words, it is proportional to the expectation value of $\langle I_z \rangle$, and is given by
124 (Keeler, 2010):

125

$$\langle I_z \rangle = \text{Tr}[\rho_0 I_z] = \frac{1}{2Z} [\exp(\hbar\omega_0/2kT) - \exp(-\hbar\omega_0/2kT)] \quad (5)$$

126

127 Hence, the Zeeman polarization for an ensemble of nuclear spins is the normalized *imbalance* between the
128 populations of the $|\alpha\rangle$ and $|\beta\rangle$ states, p_α and p_β , respectively; in other words, it is the normalized net population
129 difference that is given by:

130

$$P = \frac{p_\alpha - p_\beta}{p_\alpha + p_\beta} \quad (6)$$

131

132 This normalization is carried out with respect to the total population of the nuclear ensemble such that $p_\alpha + p_\beta =$
133 1. Therefore, the bounds on the polarization are $-1 < P < +1$. At room temperature (~ 298 K), and in a field of
134 11.75 T (500 MHz for ¹H nuclei), the thermal equilibrium Zeeman polarization, $P_{z,eq}$, is a mere $\sim 4 \times 10^{-5}$. Thus,
135 there is only a tiny population difference between the spin states of a nuclear ensemble that implies inherently
136 weak polarization. It is this small population imbalance which is manipulated in NMR experiments under thermal
137 equilibrium conditions. This weak polarization is a consequence of the small difference in energy (~ 0.1 J mol⁻¹)
138 between nuclear spin energy levels at room temperature (~ 2.5 kJ mol⁻¹); and it implies only weak alignment of
139 nuclear spins in the static magnetic field of all contemporary superconducting magnets.

140

141 In the usual quantum mechanical analysis of multiple spin systems, the density operator (that describes
142 the probability density of states) is normalized to 1, meaning that the summed (total) probability density of all
143 states is 1. This is expressed mathematically as $\text{Tr}[\rho] = 1$, where Tr denotes the trace of the matrix (Hore et al.,
144 2015). To describe non-equilibrium reactions in terms of solute concentrations requires a scaled density operator
(Kuhne et al., 1979):



145

$$\sigma_i = [A_i]\rho_i \quad , \quad (7)$$

146

147 where σ_i is now proportional to $[A_i]$. Differentiation of Eq. (7) leads to:

148

$$\frac{d\sigma_i}{dt} = [A_i]\frac{d\rho_i}{dt} + \frac{d[A_i]}{dt}\rho_i \quad . \quad (8)$$

149

150 Therefore, it follows that for a system at chemical equilibrium $d[A_i]/dt = 0$, so the scaled density operator is
151 directly proportional to the normalised density operator. For non-equilibrium systems the concentrations are time
152 dependent *viz.*, $d[A_i]/dt \neq 0$ so the two no longer scale in a straightforward manner.

153 On the other hand, equilibrium magnetization ($M_{z,eq}$) is a bulk property that is the net magnetic dipole
154 moment per unit volume; and is proportional to $\langle I_z \rangle$ where the proportionality factor is $N\hbar\gamma$. From Eq. (5) this
155 yields the expression for the magnetization in terms of magnetic field strength, temperature and number of spins
156 in the sample (or more specifically in the detection volume of the NMR spectrometer):

157

$$M_{z,eq} = \frac{N\hbar\gamma}{2} \tanh\left(\frac{\hbar\gamma B_0}{2kT}\right) \quad . \quad (9)$$

158

159 In the so-called 'high temperature limit' (room temperature, in the cases addressed here) Eq. (9) simplifies to:

160

$$M_{z,eq} = \frac{N\hbar^2\gamma^2 B_0}{4kT} \quad . \quad (10)$$

161

162 In words, 'thermal magnetization' is proportional to the magnitude of the external magnetic field strength, B_0 ,
163 and is inversely proportional to the temperature, T , while being proportional to the number of spins, N . Therefore,
164 it is *proportional* to the concentration $[A_i]$ of the solute that bears the NMR-active nucleus.

165

166 2 Equation of motion – the Bloch equations

167 In the absence of intermolecular binding (however transient), or scalar couplings, the motion (time
168 evolution) of magnetizations is described by the Bloch equations. Magnetization is explicitly declared to be
169 proportional to reactant concentrations $[A]$ and $[B]$, as has recently been discussed (Kuchel and Shishmarev,
170 2020). To explore this situation, we start with the basic Bloch equations for a single spin-1/2 ensemble. The
171 equation describes the time evolution of x , y and z magnetization in the rotating frame, and includes the influence
172 of chemical shift, RF fields, and transverse (T_2) and longitudinal relaxation (T_1) time constants. The Bloch
173 equations in their complete form are described as being inhomogeneous, and they can be written using a matrix
174 and vectors:

175



$$\frac{d}{dt} \begin{bmatrix} M_x \\ M_y \\ M_z \end{bmatrix} = - \begin{bmatrix} R_2 & \Omega & -\omega_y \\ -\Omega & R_2 & \omega_x \\ \omega_y & -\omega_x & R_1 \end{bmatrix} \begin{bmatrix} M_x \\ M_y \\ M_z \end{bmatrix} + \begin{bmatrix} 0 \\ 0 \\ R_1 M_{z,eq} \end{bmatrix}, \quad (11)$$

176

177 where $\Omega = \omega_0 - \omega_{RF}$ is the ‘offset frequency’ in the rotating frame; ω_0 (rad s⁻¹) is the Larmor frequency; ω_{RF}
 178 (rad s⁻¹) is the RF frequency; the x component of the RF field (rad s⁻¹) is $\omega_x = -\gamma B_1 \cos(\omega_{RF}t + \varphi)$; and the y
 179 component is $\omega_y = -\gamma B_1 \sin(\omega_{RF}t + \varphi)$, where the magnitude of the field strength is B_1 , and the phase of the
 180 wave form relative to an internal reference source is φ . The longitudinal relaxation rate constant is denoted by
 181 $R_1 = 1/T_1$; the transverse one by $R_2 = 1/T_2$; and the equilibrium magnetization by $M_{z,eq}$.

182 Equation (11) is tedious to solve analytically, but it is readily solved numerically (Allard et al., 1998;
 183 Helgstrand et al., 2000). On the other hand, by including the identity operator in the basis set and adding a constant
 184 to the equilibrium magnetization (Levitt and Dibari, 1992), we obtain a much more compliant (to analysis) matrix
 185 equation:

186

$$\frac{d}{dt} \begin{bmatrix} \frac{E}{2} \\ M_x \\ M_y \\ M_z \end{bmatrix} = - \begin{bmatrix} 0 & 0 & 0 & 0 \\ 0 & R_2 & \Omega & -\omega_y \\ 0 & -\Omega & R_2 & \omega_x \\ -2\theta & \omega_y & -\omega_x & R_1 \end{bmatrix} \begin{bmatrix} \frac{E}{2} \\ M_x \\ M_y \\ M_z \end{bmatrix}, \quad (12)$$

187

188 where E is equal to 1 and the factor $\theta = R_1 M_{z,eq}$ describes the equilibrium magnetization.

189

190 2.1 Chemical exchange kinetics of systems prior to and at equilibrium – the Bloch-McConnell equations

191 We can extend the system of equations from describing an ensemble of single spins to two or more
 192 exchanging spins. The system of equations now accounts for the magnetization interaction with the lattice and
 193 exchange via the forward and reverse chemical reactions. These are the Bloch-McConnell equations (McConnell,
 194 1958).

195 First, consider the rate expressions for a simple bi-directional chemical reaction. The coupled differential
 196 equations describing first-order reaction kinetics of solute A becoming solute B and back again, $A \leftrightarrow B$, are
 197 typically expressed in terms of molar concentrations:

198

$$\frac{d[A(t)]}{dt} = -k_1[A(t)] + k_{-1}[B(t)] \quad , \quad (13)$$

$$\frac{d[B(t)]}{dt} = k_1[A(t)] - k_{-1}[B(t)] \quad , \quad (14)$$

199

200 that can be expressed in matrix form:

201

$$\frac{d}{dt} \begin{bmatrix} [A(t)] \\ [B(t)] \end{bmatrix} = \begin{bmatrix} -k_1 & k_{-1} \\ k_1 & -k_{-1} \end{bmatrix} \begin{bmatrix} [A(t)] \\ [B(t)] \end{bmatrix} \quad . \quad (15)$$



202

203 The rate constant for the forward reaction is denoted by k_1 while for the reverse reaction it is k_{-1} . The time
 204 dependent concentrations are given by $[A(t)]$ and $[B(t)]$. As required by the fact that this is a closed system, the
 205 equations must conform to the *principle of conservation of mass*. Specifically, the sum of the rates of change of
 206 $[A(t)]$ and $[B(t)]$ given by $d[A(t)]/dt + d[B(t)]/dt$, is zero. We return to this point below. In other words,
 207 mass is neither created nor destroyed during the reaction in such a closed system.

208 For the simplest case of two magnetically active solutes, each possessing a single spin- $1/2$ nuclide, in
 209 chemical exchange, $A \leftrightarrow B$, the direct product (a mathematical operation used in quantum mechanics to generate
 210 the necessary combinations of states) of the chemical (solute) space $\{[A], [B]\}$ and the magnetization vector space
 211 $\{M_x, M_y, M_z\}$ for each of A and B is given by:

212

$$\begin{bmatrix} 1 \\ 1 \end{bmatrix} \otimes \begin{bmatrix} M_x \\ M_y \\ M_z \end{bmatrix} = \begin{bmatrix} M_x^A \\ M_y^A \\ M_z^A \\ M_x^B \\ M_y^B \\ M_z^B \end{bmatrix}. \quad (16)$$

213

214 A new exchange matrix in the basis of the new magnetization space $\{M_x^A, M_y^A, M_z^A, M_x^B, M_y^B, M_z^B\}$ is calculated by
 215 taking the direct product of the exchange matrix with the identity operator I that is chosen to have the same
 216 dimensions as the magnetization space. The direct product is given by:

217

$$\begin{bmatrix} -k_1 & k_{-1} \\ k_1 & -k_{-1} \end{bmatrix} \otimes \begin{bmatrix} 1 & 0 & 0 \\ 0 & 1 & 0 \\ 0 & 0 & 1 \end{bmatrix} = \begin{bmatrix} -k_1 & 0 & 0 & k_{-1} & 0 & 0 \\ 0 & -k_1 & 0 & 0 & k_{-1} & 0 \\ 0 & 0 & -k_1 & 0 & 0 & k_{-1} \\ k_1 & 0 & 0 & -k_{-1} & 0 & 0 \\ 0 & k_1 & 0 & 0 & -k_{-1} & 0 \\ 0 & 0 & k_1 & 0 & 0 & -k_{-1} \end{bmatrix}. \quad (17)$$

218

219 Likewise, the matrix describing coherent and incoherent magnetization interactions can be recast in a similar
 220 fashion to give:

221

$$\begin{bmatrix} 1 & 0 \\ 0 & 1 \end{bmatrix} \otimes \begin{bmatrix} R_2 & \Omega & -\omega_y \\ -\Omega & R_2 & \omega_x \\ \omega_y & -\omega_x & R_1 \end{bmatrix} = \begin{bmatrix} R_2^A & \Omega^A & -\omega_y & 0 & 0 & 0 \\ -\Omega^A & R_2^A & \omega_x & 0 & 0 & 0 \\ \omega_y & -\omega_x & R_1^A & 0 & 0 & 0 \\ 0 & 0 & 0 & R_2^B & \Omega^B & -\omega_y \\ 0 & 0 & 0 & -\Omega^B & R_2^B & \omega_x \\ 0 & 0 & 0 & \omega_y & -\omega_x & R_1^B \end{bmatrix}. \quad (18)$$

222

223 The inhomogeneous form of the Bloch equations can now be constructed to take into account both the coherent
 224 and incoherent interactions, *as well as* chemical exchange. This yields the inhomogeneous form of the Bloch-
 225 McConnell equations, which are written (again in matrix form) as:

226



$$\frac{d}{dt} \begin{bmatrix} M_x^A \\ M_y^A \\ M_z^A \\ M_x^B \\ M_y^B \\ M_z^B \end{bmatrix} = \begin{bmatrix} R_2^A + k_1 & \Omega^A & -\omega_y & -k_{-1} & 0 & 0 \\ -\Omega^A & R_2^A + k_1 & \omega_x & 0 & -k_{-1} & 0 \\ \omega_y & -\omega_x & R_1^A + k_1 & 0 & 0 & -k_{-1} \\ -k_1 & 0 & 0 & R_2^B + k_{-1} & \Omega^B & -\omega_y \\ 0 & -k_1 & 0 & -\Omega^B & R_2^B + k_{-1} & \omega_x \\ 0 & 0 & -k_1 & \omega_y & -\omega_x & R_1^B + k_{-1} \end{bmatrix} \begin{bmatrix} M_x^A \\ M_y^A \\ M_z^A \\ M_x^B \\ M_y^B \\ M_z^B \end{bmatrix} + \begin{bmatrix} 0 \\ 0 \\ R_1^A M_{z,eq}^A \\ 0 \\ 0 \\ R_1^B M_{z,eq}^B \end{bmatrix}, \quad (19)$$

227

228 where $M_{z,eq}^A$ and $M_{z,eq}^B$ denote the respective equilibrium magnetizations (hence the subscript *eq*).

229 The inhomogeneous form of the Bloch-McConnell equations can similarly be modified by incorporating
 230 the equilibrium magnetization to create a homogeneous form of this master equation:

231

$$\frac{d}{dt} \begin{bmatrix} \frac{E}{2} \\ M_x^A \\ M_y^A \\ M_z^A \\ M_x^B \\ M_y^B \\ M_z^B \end{bmatrix} = \begin{bmatrix} 0 & 0 & 0 & 0 & 0 & 0 & 0 \\ 0 & R_2^A + k_1 & \Omega^A & -\omega_y & -k_{-1} & 0 & 0 \\ 0 & -\Omega^A & R_2^A + k_1 & \omega_x & 0 & -k_{-1} & 0 \\ -2\theta^A & \omega_y & -\omega_x & R_1^A + k_1 & 0 & 0 & -k_{-1} \\ 0 & -k_1 & 0 & 0 & R_2^B + k_{-1} & \Omega^B & -\omega_y \\ 0 & 0 & -k_1 & 0 & -\Omega^B & R_2^B + k_{-1} & \omega_x \\ -2\theta^B & 0 & 0 & -k_1 & \omega_y & -\omega_x & R_1^B + k_{-1} \end{bmatrix} \begin{bmatrix} \frac{E}{2} \\ M_x^A \\ M_y^A \\ M_z^A \\ M_x^B \\ M_y^B \\ M_z^B \end{bmatrix}. \quad (20)$$

232

233 Again, the factors $\theta^A = R_1^A M_{z,eq}^A$ and $\theta^B = R_1^B M_{z,eq}^B$ account for the respective equilibrium magnetizations.

234

235 2.1.1 Simulations of thermal kinetics using Eq. (19)

236 Next, consider Eq. (19) for simulating the evolution of the *x*, *y*, and *z* components of the magnetization of a
 237 ‘thermal magnetization’ (*non-hyperpolarized*) sample. We seek the NMR spectrum that results from a two-site
 238 exchange reaction between solutes A and B, Fig. 1(a), as conventionally observed in room temperature NMR
 239 experiments.

240 Simulations were performed in *MatLab* with an initial equilibrium magnetization of $\mathbf{M}_0 = \mathbf{M}_{eq} =$
 241 $[0, 0, 1.0, 0, 0, 0, 0.8]$ where $M_{z,eq}^A = 1.0$ and $M_{z,eq}^B = 0.8$ are the respective equilibrium *z* magnetizations. Chemical
 242 shifts offsets were $\Omega^A = 10 \times 2 \pi \text{ rad s}^{-1}$ and $\Omega^B = 10 \times 2 \pi \text{ rad s}^{-1}$. Relaxation rate constants were $R_1^A = R_1^B =$
 243 1 s^{-1} and $R_2^A = R_2^B = 1 \text{ s}^{-1}$. The influence of an RF_{*y*} pulse was then calculated with $\omega_x = -\gamma B_1 \cos(\pi/2)$ and
 244 $\omega_y = -\gamma B_1 \sin(\pi/2)$ and with a field strength of 1.5 kHz, corresponding to $\omega_y = -\gamma B_1 = -1500 \times 2 \pi \text{ rad s}^{-1}$
 245 and $\omega_x = 0$. For a 90° RF nutation (flip) angle the pulse duration is $t_p = \pi/2\omega_y$, which gave a transformed
 246 magnetization vector after the pulse of $M(t) = [0.999, 0.007, 0.000, 0.800, -0.005, 0.000]$; this was composed
 247 mostly of $M_x^A + M_x^B$ with a residual contribution from $M_y^A + M_y^B$ arising from evolution of the chemical shift
 248 during the RF pulse; and a small contribution from $M_z^A + M_z^B$ due to return of the magnetization to the equilibrium
 249 state.

250 The observable signal (the FID, which is a function of time) is proportional to the complex signal $S(t) =$
 251 $M_x^A(t) - iM_y^A(t) + M_x^B(t) - iM_y^B(t)$. Noise was simulated by adding to the FID a normally distributed complex
 252 random vector with mean = 0 and standard deviation (SD) = 0.1. The spectrum $s(\omega)$ was then calculated by taking

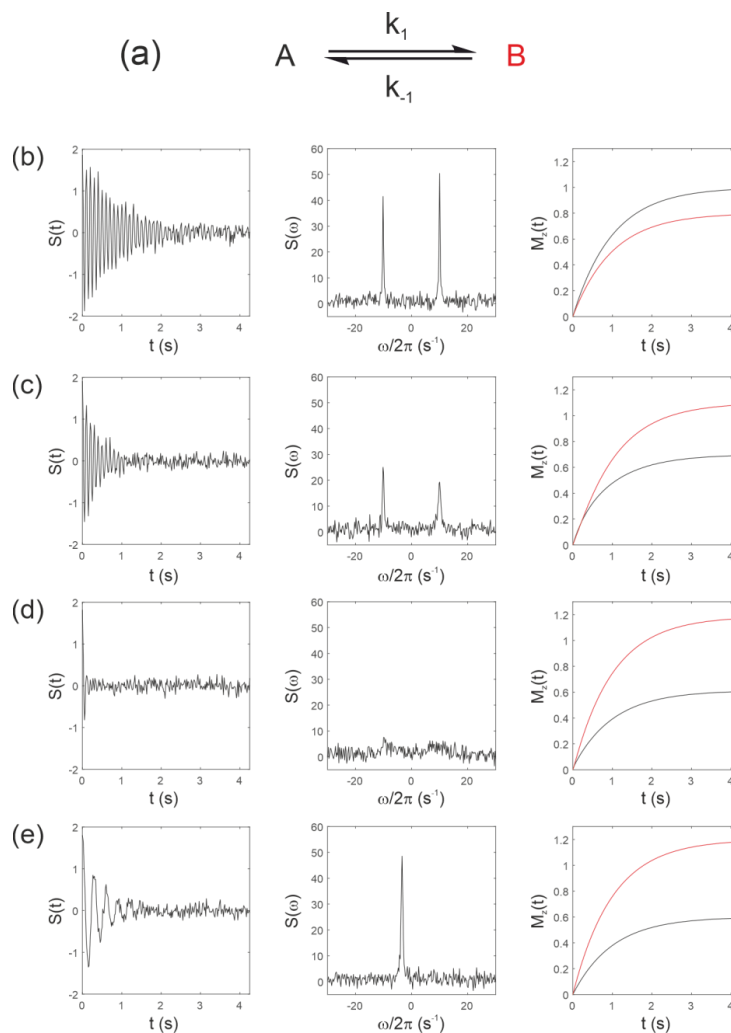


Figure 1 Simulated NMR spectra resulting from a two-site exchange process between *thermally polarized* solutes, $A \leftrightarrow B$, shown schematically in (a). Simulated FIDs $S(t)$ are shown in (b-e) left panel, with corresponding spectra $s(\omega)$, middle panel, and the recovery of z magnetizations, $M_z^A(t)$ and $M_z^B(t)$, right panel. Spectra were simulated with rate constants, (b) $k_1 = k_{-1} = 0$; (c) $k_1 = 2 \text{ s}^{-1}$, $k_{-1} = 1 \text{ s}^{-1}$; (d) $k_1 = 20 \text{ s}^{-1}$, $k_{-1} = 10 \text{ s}^{-1}$; and (e) $k_1 = 2000 \text{ s}^{-1}$, $k_{-1} = 1000 \text{ s}^{-1}$, corresponding to no exchange, slow, intermediate, and fast exchange regimes, respectively.

253 the Fourier transform of $S(t)$. Simulated FIDs $S(t)$ are shown in Figs. 1(b-e) left panel, the corresponding spectra
 254 $s(\omega)$ in Figs. 1(b-e) middle panel, and the recovery of the z magnetizations $M_z^A(t)$ and $M_z^B(t)$ are shown in Figs.
 255 1(b-e), right panel. Spectra were simulated for a range of rate constants, where exchange was either absent $k_1 =$
 256 $k_{-1} = 0$, Fig. 1(b); or for increasing rates of exchange. Thus, (c) $k_1 = 2 \text{ s}^{-1}$, $k_{-1} = 1 \text{ s}^{-1}$; (d) $k_1 = 20 \text{ s}^{-1}$,
 257 $k_{-1} = 10 \text{ s}^{-1}$; and (e) $k_1 = 2000 \text{ s}^{-1}$, $k_{-1} = 1000 \text{ s}^{-1}$, corresponding to the slow, intermediate and fast
 258 regimes, respectively.



259

260 The equilibrium constant was fixed so that $K = k_1/k_{-1} = 2$; hence the system was not at chemical
261 equilibrium at $t = 0$ s. The simulations highlight an important point: In the absence of exchange the Bloch-
262 McConnell equations predict the recovery of the z magnetizations back to their equilibrium values $M_{z,eq}^A$ and $M_{z,eq}^B$
263 while under conditions of fast exchange this no longer holds, and a non-equilibrium system will rapidly return to
264 its chemical equilibrium, not to its thermal equilibrium, within the timescale of the NMR experiment; specifically
265 within five T_1 values.

266

267 2.2 Describing hyperpolarized kinetics with the Bloch-McConnell equations

268 We now consider the predictions made by using Eq. (19) when simulating the evolution of the x , y , and
269 z components of the magnetization of a hyperpolarized sample and the resulting spectrum for a two-site exchange
270 reaction between solutes A and B. In the previous example the initial condition was $M_z^A(0) = 1.0$ and $M_z^B(0) =$
271 0.8 . To extend the Bloch-McConnell formalism to be able to predict the dynamics of a hyperpolarized experiment
272 we recognize that for the same magnitude of noise in the receiver circuit (although this may not be true for a
273 hyperpolarized sample) the initial hyperpolarized magnetization is given by:

274

$$M_{z,hyp} = \eta M_{z,eq} \quad , \quad (21)$$

275

276 where η is the enhancement factor that varies from one hyperpolarization experiment to another. In the case of
277 dDNP experiments $\eta \cong 10^4$ is typical, although this depends on the method of hyperpolarization, the solute(s) in
278 question and a set of physicochemical parameters that are described in detail in e.g., (Ardenkjaer-Larsen et al.,
279 2015).

280

281 2.2.1 Simulations of hyperpolarized kinetics using Eq. (19)

282 These were performed with an initial magnetization vector $\mathbf{M}(0) = [0.0, 1.0 \times 10^4, 0, 0, 0]$ while the
283 equilibrium magnetizations were $M_{z,eq}^A = 1.0$ and $M_{z,eq}^B = 0.8$, as used above. This situation corresponds to an
284 initial hyperpolarized magnetization $M_{z,hyp}^A(0)$ of only solute A. Chemical shifts were $\Omega^A = 10 \times 2\pi$ rad s^{-1} and
285 $\Omega^B = -10 \times 2\pi$ rad s^{-1} , while relaxation times were increased to represent a hyperpolarized ^{13}C substrate, $R_{1A} =$
286 $R_{1B} = 1/60$ s $^{-1}$ and $R_{2A} = R_{2B} = 1$ s $^{-1}$ with the rate constants representing an enzyme mediated cell reaction
287 $k_1 = k_{-1} = 0.005$ s $^{-1}$. Figure 2(a) shows the time evolution of the z -components of the magnetization, displaying
288 the familiar (Day et al., 2007) bi-exponential time dependence of $M_{z,hyp}^A(t)$ and $M_{z,hyp}^B(t)$ magnetizations.

289 We next simulate the effect of applying the pulse sequence shown in Fig. 2(b) corresponding to a time
290 course type of experiment with multiple sampling of the magnetization and acquisition of an FID at each time-
291 point. This is representative of real experiments that have been presented in the literature (Gabellieri et al., 2008;
292 Hill et al., 2013b). The time delays correspond to a pre-scan delay τ , the duration of the pulse t_p and the duration
293 of the FID t_{aq} . The experiment is repeated n times to sample the entire time course where the temporal resolution
294 is then given by the total repetition time $TR = \tau + t_p + t_{aq}$ and the total duration of the experiment is given by

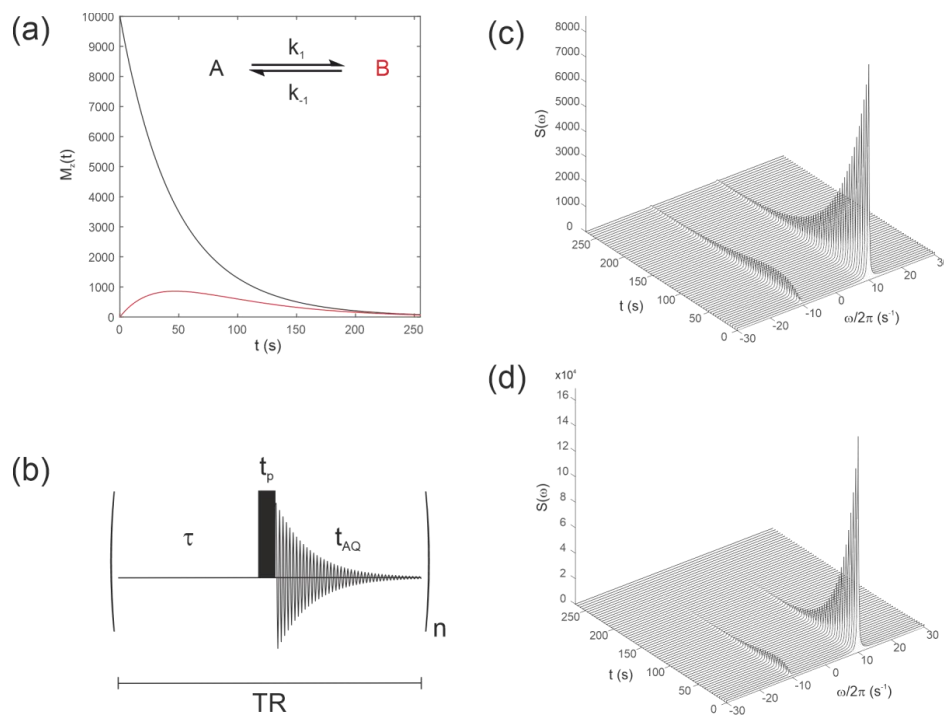


Figure 2 (a) Simulated evolution of the z -components of the magnetization M_z^A and M_z^B for a *hyperpolarized* solute $M_z^A(0) = 1 \times 10^4$ undergoing a two-site exchange reaction, $A \leftrightarrow B$. Longitudinal relaxation rate constants were $R_{1A} = R_{1B} = 1/60\text{s}^{-1}$ and $R_{2A} = R_{2B} = 1\text{s}^{-1}$. Rate constants were $k_1 = k_{-1} = 0.005\text{s}^{-1}$. (b) Simple pulse sequence for acquiring a time course experiment with multiple sampling of the magnetization and acquisition of an FID at each timepoint. (c-d) Waterfall plots of simulated spectra resulting from sequential application of the pulse sequence in (b) for an initial hyperpolarized solute A undergoing two-site exchange with solute B, calculated with a flip angles: (c) $\beta = 1^\circ$; and (d) $\beta = 20^\circ$.

295 nTR . In this experiment we make the assumption that the transverse magnetization from one experiment to the
 296 next is not recovered by the application of a subsequent pulse. This assumption is reasonable provided the
 297 acquisition time is much longer than the time taken for the FID to decay to zero, namely, $t_{aq} \gg T_2^*$.

298 The influence of this pulse sequence was then calculated, accounting for multiple sampling of the
 299 magnetization. The RF pulse was again specified by $\omega_x = -\gamma B_1 \cos(\pi/2)$ and $\omega_y = -\gamma B_1 \sin(\pi/2)$ with a field
 300 strength of 1.5 kHz, which corresponds to $\omega_y = -\gamma B_1 = -1500 \times 2\pi \text{ rad s}^{-1}$. Application of an RF pulse tilts
 301 the hyperpolarized magnetization away from the z axis by an angle of β radians. The magnitude of the observable
 302 transverse magnetization is proportional to $\sin(\beta)$, and the remaining longitudinal magnetization is proportional
 303 to $\cos(\beta)$.

304 Simulations were performed with the same magnitude of noise as in Fig. 1. The time evolution of the
 305 magnetization was recorded for the pulse sequence shown in Fig. 2(b) with sequential acquisition of 64 spectra,
 306 and a repetition time of $TR = 4.25\text{ s}$. The effect of acquiring a time series of spectra with either a flip angle $\beta =$



307 1° , Fig. 2(c), or $\beta = 20^\circ$, Fig. 2(d), are seen in the stack plots. The pulse length (duration) was $t_p = \beta \pi / 180 \omega_y$.
308 After a single $\beta = 1^\circ$ pulse applied to $\mathbf{M}(0)$ the magnetization vector was tilted to become $\mathbf{M}(t) =$
309 $[0.174, 0.000, 9.998, 0.000, 0.000, 0.000] \times 10^3$ prior to acquisition of the FID. This was composed mostly of
310 M_z^A with a small contribution from M_x^A that arose from excitation by the $\beta = 1^\circ$ pulse; or following a $\beta = 20^\circ$ pulse
311 the magnetization vector was tilted to become $\mathbf{M}(t) = [3.420, 0.004, 9.397, 0.000, 0.000, 0.000] \times 10^3$, again
312 comprised mostly of M_z^A but with a greater contribution from M_x^A due to excitation by a pulse with larger value of
313 β . Since the magnetization relaxed to its thermal equilibrium state, the hyperpolarized magnetization was
314 effectively destroyed during application of the RF (sampling) pulse, and it was not re-generated. This may not be
315 the outcome when non-linear effects such as radiation damping cause recovery of the hyperpolarized signal
316 (Weber et al., 2019).

317 The z magnetization after the application of a single RF pulse and delay TR is therefore given by:

318

$$S(TR) = S(0) \cos(\theta) \exp(-R_1 TR) \quad . \quad (22)$$

319

320 Following the application of a series of n RF pulses with a total delay $n TR = t$ the signal is given by (Kuchel
321 and Shishmarev, 2020):

322

$$S(t) = S(0) \cos^n(\theta) \exp(-R_1 t) \quad . \quad (23)$$

323

324 The apparent relaxation time constant of the hyperpolarized signal, including the influence of both the intrinsic
325 T_1 and flip angle correction, is given by (Hill et al., 2013b; Kuchel and Shishmarev, 2020):

326

$$\exp(-R_{1,app} t) = \cos^n(\theta) \exp(-R_1 t) \quad , \quad (24)$$

$$R_{1,app} = R_1 - \frac{1}{TR} \ln \cos(\theta) \quad . \quad (25)$$

327

328 In the previous examples in Figs. 2(c) and 2(d), with a typical $T_1 = 60$ s (Keshari and Wilson, 2014)
329 corresponding to $R_1 = 1.67 \times 10^{-2} \text{ s}^{-1}$ and a $TR = 4.25$ s, the flip angle correction for a $\beta = 1^\circ$ pulse was 3.58
330 $\times 10^{-5}$, which ‘for all intents and purposes’, is negligible, giving $R_{1,app} = 1.67 \times 10^{-2} \text{ s}^{-1}$ and $T_{1,app} = 59.87$ s.
331 Hence, the time dependence of the signal shown in Fig. 2(c) is a robust reflection of the $M_z(t)$ seen in Fig. 2(a).
332 For $\beta = 20^\circ$ the flip angle correction was 1.46×10^{-2} giving $R_{1,app} = 3.13 \times 10^{-2} \text{ s}^{-1}$ and $T_{1,app} = 31.95$ s.
333 Therefore, for the larger flip angle there was a tradeoff between the increased sensitivity and the corresponding
334 reduction in $T_{1,app}$ with the more rapid decay of the NMR signal. The time dependence seen in Fig. 2(d) is no
335 longer a good reflection of the $M_z(t)$ shown in Fig. 2(a). We conclude that when the RF flip angle is small, $< 1^\circ$,
336 and the magnetization is sampled many times, the flip angle correction is negligible; accordingly, it is ignored in
337 the next sections.

338



339 **3 Relaxation of hyperpolarized magnetization in ^{13}C substrates**

340 We now take a detour into relaxation theory to give an overview of the factors that determine the values
341 of $R_1 = 1/T_1$ of hyperpolarized ^{13}C solutes in a (bio)chemical system taking into account the main relaxation
342 mechanisms responsible for the decay of the nuclear magnetization in solution state at temperatures between ~20
343 to 180°C and static magnetic field strengths between 1 mT to 23.5 T. The spin interactions discussed here are
344 relevant to the outcome of numerous dissolution-dynamic nuclear polarization (dDNP) experiments.

345 A master equation for spin systems far from equilibrium based on a Lindblad dissipator formalism has
346 recently been presented and shown to correctly predict the spin dynamics of hyperpolarized systems (Bengs and
347 Levitt, 2020). In brief, Eq. (2) is only valid for the high temperature limit and weak order approximation of a spin
348 system at thermal equilibrium, and therefore the theory accounts for a dependence of relaxation rate constants on
349 the extent of hyperpolarization. However, we do not pursue this line of enquiry here because for the enzyme
350 systems studied thus far with dDNP a constant value of T_1 has been statistically satisfactory in regression analyses
351 of the data (Pages et al., 2013; Shishmarev et al., 2018b).

352 Once a sufficiently high level of nuclear spin polarization has been achieved by implementing dDNP
353 methodologies (often for ^{13}C nuclei $P_C > 60\%$) a jet of superheated solvent (*e.g.*, H_2O and/or D_2O at 150-180°C)
354 is injected directly onto the hyperpolarized sample (Ardenkjaer-Larsen et al., 2003; Wolber et al., 2004). Upon
355 contact with the warm solvent, the frozen sample rapidly dissolves and is then transferred under the pressure of
356 helium gas (6-9 bar) to a separate NMR/MRI spectrometer for the detection of hyperpolarized MRS signals, or to
357 a collection/quality control point for use in biological applications (Comment and Merritt, 2014). There are several
358 potential issues related to spin relaxation during these processes; and we focus on nuclear spin relaxation in
359 solution during the sample transfer stage (*i.e.*, subject to changes in magnetic field strength) or situations where a
360 solute has an altered rotational correlation time (*i.e.*, dependence on temperature or when bound to a protein). This
361 requires an understanding of the (potentially) large variety of molecular interactions that give rise to nuclear spin
362 relaxation.

363 **Dipole-Dipole Couplings (DD).** The dominant mechanism for the relaxation of nuclear spin
364 magnetization is often the stochastic modulation of dipole-dipole interactions (couplings) to other nuclei, either
365 in the same molecule or other molecules, including the solvent, as the molecule re-orientates in solution by
366 molecular tumbling.

367 **Chemical Shift Anisotropy (CSA).** Nuclear spins resonate at different frequencies depending on the
368 chemical shielding imparted by the local electronic environment and its orientation (a tensor property). The
369 modulation of the chemical shift tensor by molecular tumbling in solution has a quadratic dependence on the
370 strength of the static magnetic field and therefore increases markedly with \mathbf{B}_0 (Kowalewski and Maler, 2019).

371 **Paramagnetic Sites.** Dissolved paramagnetic solutes (often impurities, but they can be purposely added
372 as required by the experimental design), such as radical agents that remain in the dissolution solvent, molecular
373 oxygen, and metal ions, which can be deleterious to the nuclear-spin relaxation, particularly in regions of low
374 magnetic field (Pell et al., 2019; Blumberg, 1960). However, all species can be easily scavenged by co-dissolving
375 chelating agents in the dissolution medium (Mieville et al., 2010).

376 **Scalar Relaxation of the Second Kind.** This mechanism operates when the nuclei of interest have scalar
377 couplings to neighbouring nuclei that also relax rapidly (Pileio, 2011; Kubica et al., 2014; Elliott et al., 2019). In



378 dDNP NMR experiments this relaxation mechanism is often enhanced during sample transfer steps through areas
379 of low magnetic field (Chiavazza et al., 2013; Kubica et al., 2014).

380 **Spin Rotation.** The coupling of nuclear magnetization to that of a whole molecule or to mobile parts of
381 a molecule, *e.g.*, methyl groups, can act as an efficient relaxation mechanism. This mechanism has an unusual
382 dependence on temperature with the relaxation rate usually increasing at higher temperatures (Matson, 1977).

383 **Quadrupolar.** Many molecules of interest in dDNP experiments contain either ^2H or ^{14}N nuclei. NMR
384 relaxation times of such nuclei are often <1 s, and therefore not sufficiently long to be relevant for dDNP
385 experiments. However, there are two notable exceptions in $^6\text{Li}^+$ and $^{133}\text{Cs}^+$ which have small nuclear quadrupole
386 moments and therefore have intrinsically long T_1 values (van Heeswijk et al., 2009; Kuchel et al., 2019).

387 Derivations of relaxation rate expressions are well established and based on plausible physical models.
388 For simplicity, we skip the majority of these since they are comprehensively presented by several authors
389 (Kowalewski and Maler, 2019), and instead we focus on the main results of their analyses. Assuming a two spin
390 system composed of a ^{13}C and ^1H , equations for the ^{13}C - ^1H dipole-dipole and the ^{13}C CSA contributions to the
391 ^{13}C longitudinal relaxation rate constant (R_1) are given by Keeler (Keeler, 2010):

392

393
$$R_{1,DD} = b_{HC}^2 \left[\frac{3}{20} J(\omega_C) + \frac{1}{20} J(\omega_H - \omega_C) + \frac{3}{10} J(\omega_H + \omega_C) \right] , \quad (26)$$

394

395
$$R_{1,CSA} = c^2 \left[\frac{1}{15} J(\omega_C) \right] , \quad (27)$$

396

397 where b_{HC} is the dipole-dipole coupling constant, defined as:

398

399
$$b_{HC} = \frac{\mu_0 \gamma_H \gamma_C \hbar}{4\pi r_{HC}^3} , \quad (28)$$

400

401 and c is the magnitude of the CSA assuming an axially symmetric(al) tensor given by:

402

403
$$c = \gamma_C B_0 (\sigma_{\parallel} - \sigma_{\perp}) , \quad (29)$$

404

405 where γ_H and γ_C are the magnetogyric ratios of the ^1H and ^{13}C spins, respectively, r_{HC} is the internuclear distance
406 between the ^1H and ^{13}C atoms and σ_{\parallel} and σ_{\perp} are the parallel and perpendicular components of the axially
407 symmetric(al) CSA tensor, respectively.

408 The so-called spectral density function that is a function of the Larmor frequency, ω , is:

409

410
$$J(\omega) = \frac{2\tau_c}{1+\omega^2\tau_c^2} , \quad (30)$$

411

412 where τ_c is the rotational correlation time (tumbling motion) of the re-orientating spin-bearing molecule in
413 solution. The overall longitudinal relaxation rate constant is the sum of these two dominant contributions and is
414 given by:

415
$$R_1 = R_{1,DD} + R_{1,CSA} . \quad (31)$$



416 3.1 Relaxation Analysis

417 It is important (for experimental design purposes) to note the influence that a nearby ^1H spin has on the
 418 ^{13}C nuclear T_1 . Figure 3(a) shows the calculated ^{13}C T_1 for a fixed rotational correlation time of $\tau_c = 0.4 \times 10^{-11}$ s
 419 (previously reported for glycine in saline at 310 K (Endre et al., 1983)), ^{13}C CSA $\sigma_{\parallel} - \sigma_{\perp} = -98$ ppm (previously
 420 reported for phosphoenolpyruvate (Bechmann et al., 2004)) and a magnetic field strength of $B_0 = 7$ T as a function
 421 of the ^1H - ^{13}C internuclear distance r_{HC} . Biaxiality of the CSA interaction has been ignored here. A rapid rise occurs
 422 in T_1 as the ^1H - ^{13}C internuclear separation increases. In the case of $r_{\text{HC}} = 1.09$ Å, which is typical of a ^1H - ^{13}C
 423 single bond, the ^{13}C nuclear T_1 is predicted to be ~ 11.4 s. The ^1H - ^{13}C dipole-dipole coupling constant scales with
 424 r_{HC}^{-3} , consequently, the presence of a directly bonded proton significantly shortens the relaxation time constant of
 425 the ^{13}C magnetization. Small molecules containing ^{13}C atoms that do not have directly bonded ^1H , or at least ^1H
 426 spins located at significant internuclear distances, are required. Such moieties include the carboxyl group that is
 427 present in many low molecular weight metabolites such as pyruvate, lactate, and methylglyoxal (Shishmarev et
 428 al., 2018a). At the longer ^1H - ^{13}C internuclear distance of 1.45 Å, implying a ^1H - ^{13}C dipole-dipole coupling
 429 constant of $b_{\text{HC}}/2\pi = -10.2$ kHz, a ^{13}C nuclear T_1 of ~ 60 s is predicted. At very long distances, the ^{13}C relaxation
 430 time constant will tend to that of the CSA relaxation contribution alone.

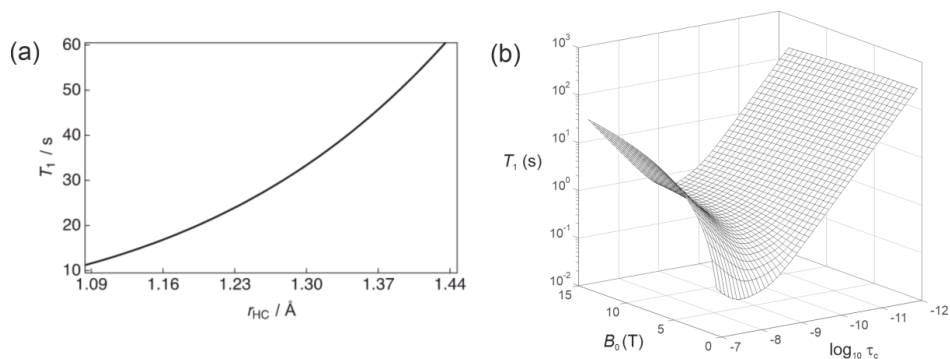


Figure 3 (a) Simulation of the ^{13}C nuclear T_1 for a two-spin ^1H - ^{13}C system as a function of the internuclear distance (r_{HC}) with a rotational correlation time $\tau_c = 0.4 \times 10^{-11}$ s, ^{13}C CSA $\sigma_{\parallel} - \sigma_{\perp} = -98$ ppm and at a magnetic field strength $B = 7$ T. (b) Dependence of the ^{13}C nuclear T_1 as a function of the magnetic field B and the rotational correlation time τ_c .

431

432 The dependence of R_1 on temperature and molecular size (*e.g.*, due to binding) scales with the rotational
 433 correlation time. Figure 3(b) shows the dependence of the ^{13}C nuclear T_1 ($1/R_1$) as a function of τ_c and B_0 for this
 434 2-spin-1/2 system with $r_{\text{HC}} = 1.45$ Å and $\sigma_{\parallel} - \sigma_{\perp} = -98$ ppm. In the extreme narrow limit, *i.e.*, $\omega^2\tau_c^2 \ll 1$, the
 435 following familiar equations describe the relaxation of ^{13}C spins under the dipole-dipole and CSA relaxation
 436 mechanisms (Kowalewski and Maler, 2019):

437

$$438 R_{1,DD} = b_{\text{HC}}^2 \tau_c \quad , \quad (32)$$

$$439 R_{1,CSA} = \frac{2}{15} c^2 \tau_c \quad . \quad (33)$$



440 In the extreme narrowing regime the ^{13}C nuclear T_1 becomes shorter with increasing magnetic field strength due
441 to the B_0^2 dependence of $R_{1,\text{CSA}}$. At low field strengths, the magnitude of T_1 will mostly be attributed to dipole-
442 dipole relaxation with the nearby ^1H spin. It is also worth noting that the ^{13}C T_1 follows the usual Lorentzian
443 spectral density functional dependence on the rotational correlation time. This is clearly seen at high magnetic
444 field.

445

446 3.2 Molecular Considerations

447 The majority of dDNP experiments used to study biological systems employ $\text{H}_2\text{O}/\text{D}_2\text{O}$ as the dissolution
448 solvent. Detection of hyperpolarized NMR/MRI signals typically occurs in a magnetic field range of 1.5-9.4 T,
449 thus Fig. 3(b) indicates a ^{13}C nuclear T_1 of the order of ~ 60 s for a carbonyl group, and this is commonly seen in
450 practice (Shishmarev et al., 2018a). It is important to remember that Eqs. (26-31) provide a greatly simplified
451 picture of the problem in hand; in reality there are many magnetic nuclei (often within the same molecule) which
452 contribute to the relaxation of ^{13}C magnetization. The additional dipole-dipole interactions are likely to be
453 responsible for differences between predicted and measured ^{13}C relaxation times, along with the other (more
454 exotic) signal attenuation mechanisms that are described above.

455 In a dDNP experiment the dissolution and transfer process can take as long as 15 s; it depends on the
456 distance to the point of use from the polarizing source; and in clinical applications an additional 30 s can easily
457 be added for quality control processes. Such requirements place a bound on the usable time in which
458 hyperpolarized ^{13}C magnetization must be maintained; and it is typical to expect 45 s to be this limit. Given that
459 the magnetic field strength “felt” by the hyperpolarized sample can be controlled (to a reasonable extent)
460 throughout its voyage between the dDNP polarizer and the point of use (Milani et al., 2015), the rotational
461 correlation time becomes the most important factor that impacts upon the ^{13}C nuclear T_1 . Figure 3(b) indicates
462 that even for a rotational correlation time on the order of $\tau_c = 1 \times 10^{-10}$ s, such as found in proteins in solution
463 (Wilbur et al., 1976), Eq. (26-31) yields ^{13}C nuclear T_1 relaxation times which are too short to allow practical use
464 of such samples, *i.e.*, $5 \times T_1 < 45$ s, in comparison to the overall time required by a dDNP experiment.

465 A major parameter that controls the magnitude of the rotational correlation time of a spin-bearing
466 molecule is its molecular weight (M_w). Since $\tau_c \propto M_w$ the rotational correlation time has a noticeable impact on
467 the ^{13}C nuclear T_1 with even the smallest increase in molecular weight. In order to achieve ^{13}C nuclear T_1 relaxation
468 times that are sufficiently long to enable hyperpolarized ^{13}C magnetization to survive the dissolution and transfer
469 process the ^{13}C NMR signals must be detectable above the spectral noise for ~ 45 s. Hence, dDNP samples used
470 in biological experiments are currently restricted to small molecules (or ions (Kuchel et al., 2019; van Heeswijk
471 et al., 2009)). For example, the estimate of ~ 60 s for the ^{13}C nuclear T_1 of the model system described above was
472 predicted with a rotational correlation time of $\tau_c = 0.4 \times 10^{-11}$ (Endre et al., 1983), and this is sufficiently long for
473 dDNP experiments.

474

475



476 3.3 Enzyme Binding

477 The worst-case scenario for the model system described in Fig. 3(b) would be a moderate rotational
478 correlation time of the order of $\tau_c = 1 \times 10^{-8} - 1 \times 10^{-10}$ s for which ^{13}C nuclear T_1 relaxation times in the millisecond
479 regime are predicted. Such correlation times correspond to a system with a molecular weight comparable to that
480 of an enzyme. If the small molecule (ligand) or ion becomes bound to the enzyme, then it will assume the rotational
481 correlation time of the higher mass binding partner. In the case of $\tau_c = 1 \times 10^{-9}$ for an enzyme-ligand complex, a
482 ^{13}C substrate will have a predicted nuclear T_1 of ~ 276.4 ms at a static magnetic field strength of 7 T. Such a stark
483 variation in ^{13}C nuclear T_1 values provides good contrast in relaxation-based ligand-protein binding experiments
484 (Valensin et al., 1982).

485

486 4 Mechanistic description of reaction kinetics of hyperpolarized substrates

487 We now consider the interpretation of hyperpolarized dynamics for complex chemical reactions. To help
488 tease apart the key features of the analysis we begin with some simplifying assumptions. First, in the absence of
489 an RF pulse Eq. (20) becomes block diagonal, since transverse and longitudinal magnetization are not
490 interconverted. The evolution of the z magnetization is then dependent only on the initial conditions, T_1 , and the
491 rate constants that characterize the chemical exchange. Second, we assume that the z magnetization is sampled
492 many times with an infinitesimally small flip angle ($\ll 1^\circ$) so the longitudinal magnetization decays with its
493 intrinsic T_1 value rather than an apparent $T_{1,app}$ value. Finally, the hyperpolarized magnetization decays to zero,
494 *i.e.*, the enhancement factor η (Eq. (21)) is such that \mathbf{M}_0 is greater than \mathbf{M}_{eq} by many orders of magnitude. Thus,
495 the equilibrium magnetization at $t = \infty$ is effectively zero and it can be ignored in the analysis of real experimental
496 data.

497 To reduce clutter in the equations, for all the discussions that now follows, we drop the subscript z since
498 we hereafter deal only with longitudinal magnetization and denote $M_{z,hyp}^A$ and $M_{z,hyp}^B$ as $A^*(t)$ and $B^*(t)$
499 corresponding to hyperpolarized magnetization (identified with an asterisk *).

500

501 4.1 Simple first order exchange kinetics of hyperpolarized substrates

502 Confining our analysis to the physical subspace that is composed of longitudinal magnetizations, which
503 describe first-order kinetics of a two-site exchange reaction of hyperpolarized substrates, $A^* \leftrightarrow B^*$, Eq. (20)
504 simplifies to:

505

$$\frac{d}{dt} \begin{bmatrix} A^*(t) \\ B^*(t) \end{bmatrix} = \begin{bmatrix} -k_1 - R_1^A & k_{-1} \\ k_1 & -k_{-1} - R_1^B \end{bmatrix} \begin{bmatrix} A^*(t) \\ B^*(t) \end{bmatrix} . \quad (34)$$

506

Equivalently, Eq. (34) can be expanded to give:

$$\frac{dA^*(t)}{dt} = -k_1 A^*(t) + k_{-1} B^*(t) - R_1^A A^*(t) , \quad (35)$$



$$\frac{dB^*(t)}{dt} = k_1 A^*(t) - k_{-1} B^*(t) - R_1^B B^*(t) \quad , \quad (36)$$

507

508 where k_1 and k_{-1} denote first-order rate constants, and $R_1^A = 1/T_1^A$ and $R_1^B = 1/T_1^B$ are the longitudinal relaxation
 509 rate constants of A and B, respectively.

510 Since Eqs. (35) and (36) describe the time evolution of the z magnetizations (that is proportional to
 511 concentration/mass) they do not satisfy the conservation of mass requirement because $d[A^*(t) + B^*(t)]/dt =$
 512 $-R_1^A A^*(t) - R_1^B B^*(t)$ and this tends to zero with time. However, the equations can be recast to specify that the
 513 pools of hyperpolarized substrates relax to form pools of non-polarized substrates $A \leftrightarrow B$. These pools are denoted
 514 simply by $A(t)$ and $B(t)$ (without the asterisks) as shown in Fig. 4(a). The analogy with radioactive tracers is a
 515 useful one here. A ‘hot’ pool of radioactive material decays with first order kinetics (half-life) to form a ‘cold’
 516 pool of non-radioactive material with the sum of ‘hot’ and ‘cold’ being constant.

517 The kinetics of the non-polarized pools are described by:

518

$$\frac{dA(t)}{dt} = -k_1 A(t) + k_{-1} B(t) + R_1^A A^*(t) \quad , \quad (37)$$

$$\frac{dB(t)}{dt} = k_1 A(t) - k_{-1} B(t) + R_1^B B^*(t) \quad . \quad (38)$$

519

520 Equations (37) and (38) now satisfy conservation of mass, since the rate of change $d[A^*(t) + A(t) + B^*(t) +$
 521 $B(t)]/dt$ is always zero. Note that $A(t)$ and $B(t)$ are not observed in the dDNP NMR experiment; but they are
 522 the counterparts of real concentrations of solute that would be assayable (bio)chemically.

523 Equations (35-38) can be written as:

524

$$\frac{d}{dt} \begin{bmatrix} A^*(t) \\ B^*(t) \\ A(t) \\ B(t) \end{bmatrix} = \begin{bmatrix} -k_1 - R_1^A & k_{-1} & 0 & 0 \\ k_1 & -k_{-1} - R_1^B & 0 & 0 \\ R_1^A & 0 & -k_1 & k_{-1} \\ 0 & R_1^B & k_1 & -k_{-1} \end{bmatrix} \begin{bmatrix} A^*(t) \\ B^*(t) \\ A(t) \\ B(t) \end{bmatrix} \quad . \quad (39)$$

525

526 We can now appreciate the equivalence between this formalism and conventional chemical reaction kinetics that
 527 are written in terms of molecular concentrations. Furthermore, Eq. (39) can be rewritten as:

528

$$\frac{d}{dt} \begin{bmatrix} A^*(t) + A(t) \\ B^*(t) + B(t) \end{bmatrix} = \begin{bmatrix} -k_1 & k_{-1} \\ k_1 & -k_{-1} \end{bmatrix} \begin{bmatrix} A^*(t) + A(t) \\ B^*(t) + B(t) \end{bmatrix} \quad , \quad (40)$$

529

530 thereby recapturing the conventional form of chemical reaction kinetics for a closed system. Therefore, $A^*(t) +$
 531 $A(t)$ and $B^*(t) + B(t)$ are proportional to $[A(t)]$ and $[B(t)]$, respectively, where the constant of proportionality
 532 depends on the initial experimental conditions, *viz.*, $[A]_0$ and $[B]_0$. In other words, provided $A^*(0) + A(0) = [A]_0$
 533 and $B^*(0) + B(0) = [B]_0$ then the constant of proportionality is 1 and we can equate $A^*(t) + A(t) = [A(t)]$ and
 534 $B^*(t) + B(t) = [B(t)]$. This is a crucial point that we return to below.

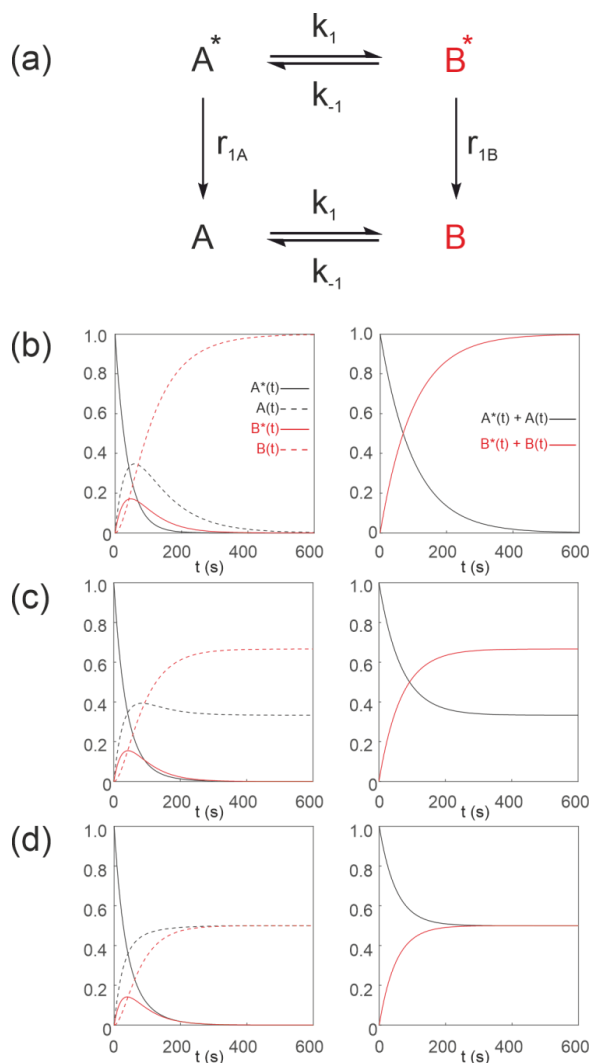


Figure 4 Simulated first order two-site exchange kinetics of hyperpolarized solutes, $A \leftrightarrow B$, conforming to conservation of mass, assuming initial hyperpolarized magnetization of only solute $A^*(0) = 1$. Longitudinal relaxation rate constants were $R_1^A = R_1^B = 1/60\text{s}^{-1}$. The time dependence of $A^*(t)$, $A(t)$, $B^*(t)$ and $B(t)$ (left panel) were calculated numerically using Eq. (35-38) with rate constants (b) $k_1 = 0.01\text{ s}^{-1}$, $k_{-1} = 0\text{ s}^{-1}$, corresponding to uni-directional kinetics, (c) $k_1 = 0.01\text{ s}^{-1}$, $k_{-1} = 0.005\text{ s}^{-1}$ and (d) $k_1 = 0.01\text{ s}^{-1}$, $k_{-1} = 0.01\text{ s}^{-1}$, corresponding to exchange kinetics. The right panel shows plots of the time dependence of $A^*(t) + A(t) = [A(t)]$ and $B^*(t) + B(t) = [B(t)]$.

535 Figure 4 shows numerical simulations of the time evolution of the system described by Eq. (39) with an
 536 initial magnetization vector $\mathbf{M}(0) = [1, 0, 0, 0]$ that corresponds to only hyperpolarized $A^*(0) = 1$ and
 537 longitudinal relaxation rate constants $R_1^A = R_1^B = 1/60\text{s}^{-1}$. The time dependence of $A^*(t)$, $A(t)$, $B^*(t)$ and $B(t)$
 538 were calculated numerically (left panel) for different rate constants: Fig. 4(b), $k_1 = 0.01\text{ s}^{-1}$, $k_{-1} = 0\text{ s}^{-1}$,



539 corresponding to a uni-directional reaction; Fig 4(c), $k_1 = 0.01 \text{ s}^{-1}$, $k_{-1} = 0.005 \text{ s}^{-1}$, corresponding to bi-directional
540 exchange with an equilibrium constant $K = 2$; and Fig. 4(d), $k_1 = 0.01 \text{ s}^{-1}$, $k_{-1} = 0.01 \text{ s}^{-1}$, also corresponding to bi-
541 directional exchange with an equilibrium constant $K = 1$. The right column shows plots of the time dependence
542 of $A^*(t) + A(t)$ and $B^*(t) + B(t)$ that reproduce conventional kinetics of $[A(t)]$ and $[B(t)]$, as required for
543 mathematical and physical consistency.

544 The approach used here (as laid out in (Kuchel and Shishmarev, 2020)) enables us to create systems of
545 differential equations that satisfy conservation of mass and therefore allow a study of the influence of non-
546 hyperpolarized pools of substrates on reaction kinetics. The approach enables more complicated reaction
547 mechanisms to be described to allow the inclusion of MR invisible pools of substrates such as ^{12}C , which are
548 known to affect the outcome of dDNP experiments *in vivo*. We consider some of these scenarios next.
549

550 4.2 Sequential reaction kinetics of hyperpolarized substrates

551 Equation 39 can be extended to compartmental models of arbitrary complexity: Consider a reaction scheme
552 involving three substrates $A^* \leftrightarrow B^* \leftrightarrow C^*$ which relax through T_1 processes to form a pool of non-polarized
553 substrates $A \leftrightarrow B \leftrightarrow C$, as shown in Fig. 5(a). This is analogous to a system where a solution of hyperpolarized
554 solute A^* is introduced into the extracellular medium in a cell suspension, is transported into the cells where it is
555 denoted by B^* and it is subsequently acted upon by an enzyme to form C^* . The system of differential equations
556 that describe the kinetics of this scheme is:

557

$$\frac{dA^*(t)}{dt} = -k_1 A^*(t) + k_{-1} B^*(t) - R_1^A A^*(t) \quad , \quad (41)$$

$$\frac{dB^*(t)}{dt} = k_1 A^*(t) - k_{-1} B^*(t) - k_2 B^*(t) + k_{-2} C^*(t) - R_1^B B^*(t) \quad , \quad (42)$$

$$\frac{dC^*(t)}{dt} = k_2 B^*(t) - k_{-2} C^*(t) - R_1^C C^*(t) \quad , \quad (43)$$

$$\frac{dA(t)}{dt} = -k_1 A(t) + k_{-1} B(t) + R_1^A A^*(t) \quad , \quad (44)$$

$$\frac{dB(t)}{dt} = k_1 A(t) - k_{-1} B(t) - k_2 B(t) + k_{-2} C(t) + R_1^B B^*(t) \quad , \quad (45)$$

$$\frac{dC(t)}{dt} = k_2 B(t) - k_{-2} C(t) + R_1^C C^*(t) \quad , \quad (46)$$

558

559 where we have removed the square brackets that denote molar concentration to avoid some of the clutter.
560 However, it is important to recall that there is a factor that relates magnetization to concentration, and this is
561 estimated from the known initial experimental conditions.

562 Equations (41-46) can be recast in matrix form to give:

563

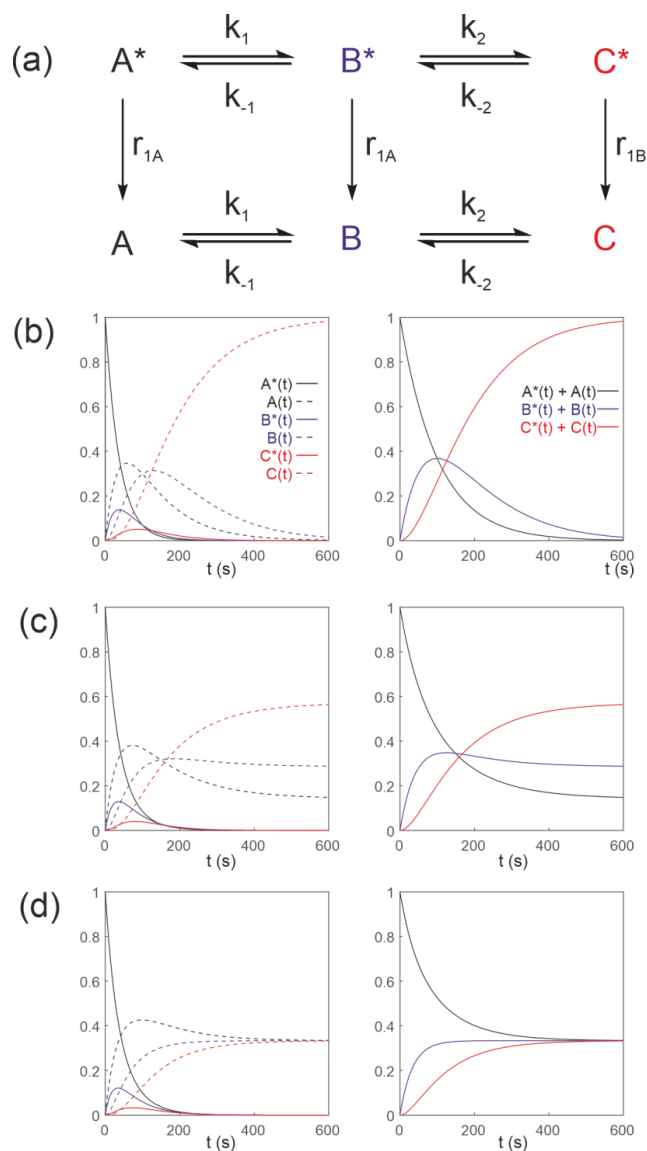


Figure 5 Simulated first order three-site exchange kinetics of hyperpolarized solutes, $A \leftrightarrow B \leftrightarrow C$, conforming to conservation of mass, assuming initial hyperpolarized magnetization of only solute $A^*(0) = 1$. Longitudinal relaxation rate constants were $R_1^A = R_1^B = R_1^C = 1/60 \text{ s}^{-1}$. The time dependence of $A^*(t)$, $A(t)$, $B^*(t)$, $B(t)$, $C^*(t)$ and $C(t)$ (left panel) were calculated numerically using Eq. (41-46) with rate constants (b) $k_1 = k_2 = 0.01 \text{ s}^{-1}$, $k_{-1} = k_{-2} = 0 \text{ s}^{-1}$, corresponding to uni-directional kinetics, (c) $k_1 = k_2 = 0.01 \text{ s}^{-1}$, $k_{-1} = k_{-2} = 0.005 \text{ s}^{-1}$ and (d) $k_1 = k_2 = k_{-1} = k_{-2} = 0.01 \text{ s}^{-1}$, corresponding to exchange kinetics. The right panel shows plots of the time dependence of $A^*(t) + A(t) = [A(t)]$, $B^*(t) + B(t) = [B(t)]$ and $C^*(t) + C(t) = [C(t)]$.



$$\frac{d}{dt} \begin{bmatrix} A^*(t) \\ B^*(t) \\ C^*(t) \\ A(t) \\ B(t) \\ C(t) \end{bmatrix} = \begin{bmatrix} -k_1 - R_1^A & k_{-1} & 0 & 0 & 0 & 0 \\ k_1 & -k_{-1} - k_2 - R_1^B & k_{-2} & 0 & 0 & 0 \\ 0 & k_2 & -k_{-2} - R_1^C & 0 & 0 & 0 \\ R_1^A & 0 & 0 & -k_1 & k_{-1} & 0 \\ 0 & R_1^B & 0 & k_1 & -k_{-1} - k_2 & k_{-2} \\ 0 & 0 & R_1^C & 0 & k_2 & -k_{-2} \end{bmatrix} \begin{bmatrix} A^*(t) \\ B^*(t) \\ C^*(t) \\ A(t) \\ B(t) \\ C(t) \end{bmatrix}. \quad (47)$$

565

566 It is readily verified that Eq. (47) satisfies conservation of mass, since the rate of change $(A^*(t) + A(t) + B^*(t) +$
 567 $B(t) + C^*(t) + C(t))/dt = 0$.

568 Equations (41-46) can be re-written in matrix-vector form as:

569

$$\frac{d}{dt} \begin{bmatrix} A^*(t) + A(t) \\ B^*(t) + B(t) \\ C^*(t) + C(t) \end{bmatrix} = \begin{bmatrix} -k_1 & k_{-1} & 0 \\ k_1 & -k_{-1} - k_2 & k_{-2} \\ 0 & k_2 & -k_{-2} \end{bmatrix} \begin{bmatrix} A^*(t) + A(t) \\ B^*(t) + B(t) \\ C^*(t) + C(t) \end{bmatrix}, \quad (48)$$

570

571 Therefore, provided $A^*(0) + A(0) = [A]_0$, $B^*(0) + B(0) = [B]_0$ and $C^*(0) + C(0) = [C]_0$, then $A^*(t) +$
 572 $A(t) = [A(t)]$, $B^*(t) + B(t) = [B(t)]$ and $C^*(t) + C(t) = [C(t)]$, respectively.

573 Figure 5 shows the results of numerical integration of Eq. (47) with initial magnetization vector $\mathbf{M}(0) =$
 574 $[1, 0, 0, 0, 0, 0]$ that corresponds to having only hyperpolarized $A^*(0) = 1$ and longitudinal relaxation rate constants
 575 $R_1^A = R_1^B = R_1^C = 1/60s^{-1}$. The time dependence of $A^*(t)$, $A(t)$, $B^*(t)$, $B(t)$, $C^*(t)$ and $C(t)$ were calculated
 576 (left panel) for different rate constants: Fig. 5(b), $k_1 = k_2 = 0.01 s^{-1}$, $k_{-1} = k_{-2} = 0 s^{-1}$, corresponding to uni-
 577 directional kinetics; Fig. 5(c), $k_1 = k_2 = 0.01 s^{-1}$, $k_{-1} = k_{-2} = 0.005 s^{-1}$, corresponding to bi-directional
 578 exchange kinetics; and Fig. 5(d), $k_1 = k_2 = k_{-1} = k_{-2} = 0.01 s^{-1}$, also corresponding to bi-directional
 579 exchange kinetics. The right column shows plots of the time dependence of $A^*(t) + A(t)$, $B^*(t) + B(t)$ and
 580 $C^*(t) + C(t)$, which reproduce the conventional chemical kinetics of $[A(t)]$, $[B(t)]$ and $[C(t)]$, as required for
 581 mathematical and physical consistency.

582

583 4.3 Second-order kinetics of hyperpolarized substrates

584 We now describe hyperpolarized substrates $A^*(t)$ and $B^*(t)$ reacting with non-hyperpolarized substrates $[C(t)]$
 585 and $[D(t)]$. The system of differential equations that describes these second-order kinetics of $A^* + C \leftrightarrow B^* + D$
 586 with only the hyperpolarized pools relaxing through T_1 processes to form a pool of non-polarized substrates $A +$
 587 $C \leftrightarrow B + D$. The reactant concentrations $[C(t)]$ and $[D(t)]$ are common to both pools, as shown in Fig. 6(a). The
 588 relevant system of differential equations (again omitting the square brackets that denote concentration) is:

589

$$\frac{dA^*(t)}{dt} = -k_1 C(t) A^*(t) + k_{-1} D(t) B^*(t) - R_1^A A^*(t), \quad (49)$$

$$\frac{dB^*(t)}{dt} = k_1 C(t) A^*(t) - k_{-1} D(t) B^*(t) - R_1^B B^*(t), \quad (50)$$



$$\frac{dA(t)}{dt} = -k_1 C(t) A(t) + k_{-1} D(t) B(t) + R_1^A A^*(t) \quad , \quad (51)$$

$$\frac{dB(t)}{dt} = k_1 C(t) A(t) - k_{-1} D(t) B(t) + R_1^B B^*(t) \quad , \quad (52)$$

$$\frac{d[C(t)]}{dt} = -k_1 C(t) (A^*(t) + A(t)) + k_{-1} D(t) (B^*(t) + B(t)) \quad , \quad (53)$$

$$\frac{d[D](t)}{dt} = k_1 C(t) (A^*(t) + A(t)) - k_{-1} D(t) (B^*(t) + B(t)) \quad . \quad (54)$$

590

591 As was done above with sets of simultaneous differential equations, Eqs. (49-54) can be cast into matrix-vector
 592 form:

593

$$\frac{d}{dt} \begin{bmatrix} A^*(t) + A(t) \\ B^*(t) + B(t) \\ C(t) \\ D(t) \end{bmatrix} = \begin{bmatrix} -k_1 C(t) & k_{-1} D(t) & 0 & 0 \\ k_1 C(t) & -k_{-1} D(t) & 0 & 0 \\ -k_1 C(t) & k_{-1} D(t) & 0 & 0 \\ k_1 C(t) & -k_{-1} D(t) & 0 & 0 \end{bmatrix} \begin{bmatrix} A^*(t) + A(t) \\ B^*(t) + B(t) \\ C(t) \\ D(t) \end{bmatrix} \quad . \quad (55)$$

594

595 Again, mass is conserved as seen by the fact that $d((A^*(t) + A(t) + B^*(t) + B(t)))/dt = 0$ and $d(C(t) +$
 596 $D(t))/dt = 0$. Also, recall that provided $A^*(0) + A(0) = [A]_0$, $B^*(0) + B(0) = [B]_0$, $C(0) = [C]_0$ and $D(0) =$
 597 $[D]_0$, then we can make use of the equalities $A^*(t) + A(t) = [A(t)]$, $B^*(t) + B(t) = [B(t)]$, $C(t) = [C(t)]$ and
 598 $D(t) = [D(t)]$, respectively. It is now very evident why we must equate the initial signal with the concentration
 599 via an experimentally estimated scaling factor.

600

Figure 6 shows numerical simulations of the time evolution of the system of Eqs. (49-54) with initial
 601 magnetization corresponding to the hyperpolarized signal $A^*(0) = 1$ and non-polarized substrates $C(0) = 0.95$
 602 and $D(0) = 0.05$. The longitudinal relaxation rate constants were $R_{1A} = R_{1B} = 1/60s^{-1}$. The time dependence
 603 of $A^*(t)$, $A(t)$, $B^*(t)$ and $B(t)$ are subject to second order kinetics and were calculated numerically (left panel)
 604 for different rate constants: Fig. 6(b), $k_1 = 0.01 s^{-1}$, $k_{-1} = 0 s^{-1}$, corresponding to unidirectional kinetics; Fig.
 605 6(c), $k_1 = 0.01 s^{-1}$, $k_{-1} = 0.005 s^{-1}$, corresponding to bi-directional exchange kinetics with an equilibrium
 606 constant $K = 2$; and Fig. 6(d) $k_1 = k_{-1} = 0.01 s^{-1}$, with an equilibrium constant $K = 1$, also corresponding to bi-
 607 directional exchange kinetics. The right column shows plots of the time dependence of $A^*(t) + A(t)$, $B^*(t) +$
 608 $B(t)$, which capture conventional chemical kinetics of the concentrations of $[A(t)]$ and $[B(t)]$, as required, as
 609 well as the kinetics of the non-polarized reactants $[C(t)]$ and $[D(t)]$.

610

611 4.3.1 An Ersatz solution

612

The system of differential equations in Eq. (55), describing a second order reaction can be reduced to one with
 613 pseudo first order kinetics by introducing time-dependent rate constants $k'_1(t) = k_1 C(t)$ and $k'_{-1}(t) = k_{-1} D(t)$.
 614 Importantly, the pseudo first order rate constants $k'_1(t)$ and $k'_{-1}(t)$ are now time dependent. This approach has



615 been used previously (Mariotti et al., 2016) but it constitutes a special case of the more general method described
 616 here, which we advocate.
 617
 618

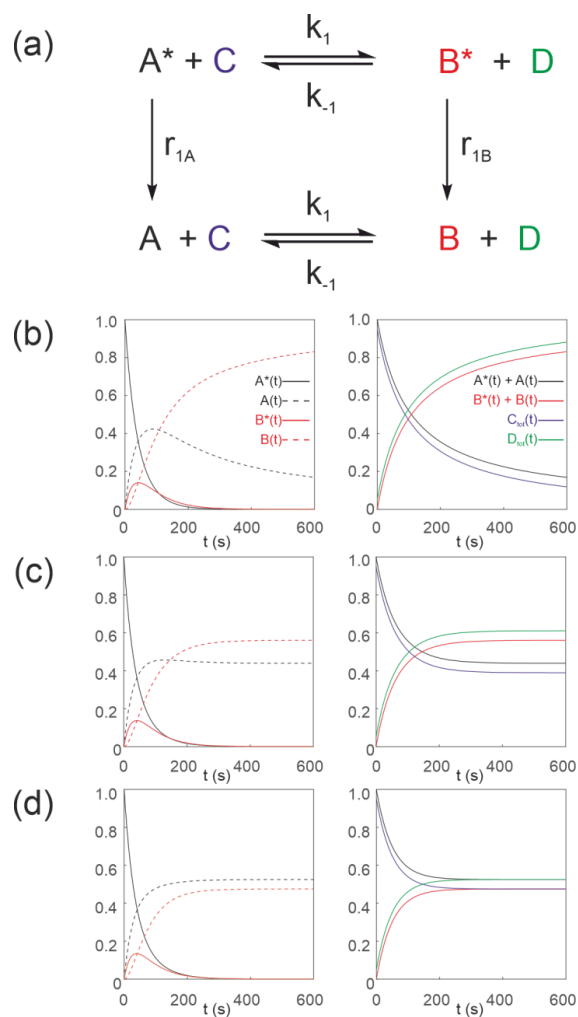


Figure 6 Simulated second order exchange kinetics of hyperpolarized solutes, $A^* + C \leftrightarrow B^* + D$, conforming to conservation of mass, assuming initial hyperpolarized magnetization of only solute $A^*(0) = 1$. Longitudinal relaxation rate constants were $R_1^A = R_1^B = 1/60 s^{-1}$. The time dependence of $A^*(t)$, $A(t)$, $B^*(t)$ and $B(t)$ were simulated (left panel) using Eqs. (49-54) with rate constants (b) $k_1 = 0.01 s^{-1}$, $k_{-1} = 0 s^{-1}$, corresponding to uni-directional kinetics (c) $k_1 = 0.01 s^{-1}$, $k_{-1} = 0.005 s^{-1}$ and (d) $k_1 = k_{-1} = 0.01 s^{-1}$, corresponding to exchange kinetics. The right panel shows plots of the time dependence of $A^*(t) + A(t) = [A(t)]$, $B^*(t) + B(t) = [B(t)]$ and non-polarized reactants $[C(t)]$ and $[D(t)]$.

619



620 **5 Michaelis-Menten equation for a hyperpolarized substrate**

621 Next consider an enzyme catalysed reaction with a hyperpolarized substrate. The simplest model
 622 involves a hyperpolarized substrate $S^*(t)$ that is in equilibrium with a free enzyme of concentration $[E]_0$ to form
 623 a hyperpolarized enzyme substrate complex $ES^*(t)$, which then reacts to form a hyperpolarized product $P^*(t)$.
 624 This is followed by release of the free enzyme that is then available for further reactions: $E + S^* \leftrightarrow ES^* \leftrightarrow P^* +$
 625 E . All hyperpolarized substrates relax through T_1 processes to form non-polarized pools of substrates $E + S \leftrightarrow ES$
 626 $\leftrightarrow P + E$ as shown in Fig. 7(a). The differential equations (again omitting the square brackets denoting
 627 concentration) that describe the reaction kinetics are:
 628

$$\frac{dS^*(t)}{dt} = -k_1E(t)S^*(t) + k_{-1}ES^*(t) - R_1^S S^*(t) \quad , \quad (56)$$

$$\frac{dS(t)}{dt} = -k_1E(t)S(t) + k_{-1}ES(t) + R_1^S S^*(t) \quad , \quad (57)$$

$$\frac{dES^*(t)}{dt} = k_1E(t)S^*(t) - k_{-1}ES^*(t) - k_2ES^*(t) + k_{-2}E(t)P^*(t) - R_1^{ES} ES^*(t) \quad , \quad (58)$$

$$\frac{dES(t)}{dt} = k_1E(t)S(t) - k_{-1}ES(t) - k_2ES(t) + k_{-2}E(t)P(t) + R_1^{ES} ES^*(t) \quad , \quad (59)$$

$$\frac{dP^*(t)}{dt} = k_2ES^*(t) - k_{-2}E(t)P^*(t) - R_1^P P^*(t) \quad , \quad (60)$$

$$\frac{dP(t)}{dt} = k_2ES(t) - k_{-2}E(t)P(t) + R_1^P P^*(t) \quad , \quad (61)$$

$$\frac{dE(t)}{dt} = -k_1E(t)(S^*(t) + S(t)) + (k_{-1} + k_2)(ES^*(t) + ES(t)) - k_{-2}E(t)(P^*(t) + P(t)) \quad , \quad (62)$$

629 where $E(t)$ is the free enzyme, $ES(t)$ is the enzyme-substrate complex, $S(t)$ is the free substrate and $P(t)$ is the
 630 free product, with relaxation rate constants R_1^S , R_1^{ES} and R_1^P , respectively. Note the appearance of the free enzyme
 631 $E(t)$ as both a reactant and product; it is regenerated through the reactions that are characterized by the rate
 632 constants k_1 and k_{-1} , and also k_2 and k_{-2} , thereby being recycled.

634 Mass is conserved as confirmed by the fact that $d(S^*(t) + S(t) + ES^*(t) + ES(t) + P^*(t) + P(t))/$
 635 $dt = 0$ and $d(ES^*(t) + ES(t) + E(t))/dt = 0$. Therefore, provided $S^*(0) + S(0) = [S]_0$, $ES^*(0) + ES(0) =$
 636 $[ES]_0$ and $P^*(0) + P(0) = [P]_0$ then $S^*(t) + S(t) = [S(t)]$, $ES^*(t) + ES(t) = [ES(t)]$ and $P^*(t) + P(t) =$
 637 $[P(t)]$, respectively.

638
 639



640 5.1 Steady state of ES complex

641 A simplified uni-directional enzyme catalysed reaction is described by setting the reverse rate constant
642 $k_{-2} = 0$ (see Fig. 7(a)). If it is assumed that a steady-state of $[ES]$ is attained very rapidly then
643 $d(ES^*(t) + ES(t))/dt = 0$ and we obtain (reverting to using square brackets to denote molar concentration):
644

$$k_1[E(t)][S^*(t) + S(t)] = (k_{-1} + k_2)[ES^*(t) + ES(t)] \quad . \quad (63)$$

645
646 Rearranging Eq. (63) yields the Michaelis constant in terms of hyperpolarized and non-polarized pools of
647 substrate:
648

$$K_M = \frac{(k_{-1} + k_2)}{k_1} = \frac{[E(t)][S^*(t) + S(t)]}{[ES^*(t) + ES(t)]} \quad . \quad (64)$$

649
650 Calibrating the signals to molar concentrations is important since the signals now relate to a real parameter (K_M)
651 of the enzyme that has units of concentration (typically mM).

652 Thus, using conservation of enzyme mass, the free enzyme concentration is given by:

$$[E(t)] = [E]_0 - [ES^*(t) + ES(t)] \quad . \quad (65)$$

654
655 Then
656

$$\frac{d([P^*(t) + P(t)])}{dt} = \frac{k_2[E]_0 [S^*(t) + S(t)]}{K_M + [S^*(t) + S(t)]} \quad . \quad (66)$$

657
658 In other words, this is the standard form of the Michaelis-Menten equation written as a function of both polarized
659 and unpolarized pools of substrate.
660

661 5.2 Simulations of Michaelis-Menten reaction

662 Figure 7(b-c) shows the results of numerical integration of Eqs. (56-62) with an initial hyperpolarized
663 signal $S^*(0) = 0.001$ (corresponding to a concentration $[S]_0 = 1$ mM via the experimentally determined scaling
664 factor, which here was set to 1) and enzyme concentration $[E]_0 = 1 \times 10^{-9}$ M. The assigned longitudinal
665 relaxation rate constants were $R_{1S} = R_{1ES} = R_{1P} = 1/60s^{-1}$. In the first instance, we set the longitudinal
666 relaxation times of substrate, enzyme-substrate complex and product to be equal (this is discussed further below).
667 The reaction rate constants were $k_1 = 1 \times 10^7 s^{-1}$, $k_{-1} = 1 \times 10^2 s^{-1}$, $k_2 = 5 \times 10^3 s^{-1}$, $k_{-2} = 0 s^{-1}$, such
668 that $K_M = 5.1 \times 10^{-4}$ M and $V_{max} = 5 \times 10^{-6}$ M s^{-1} . The time dependences of $S^*(t)$, $S(t)$, $P^*(t)$ and $P(t)$ are
669 shown in Fig. 7(b), left panel, subject to standard uni-directional Michaelis-Menten kinetics; and in Fig. 7(c), left
670 panel, the time dependence of $ES^*(t)$ and $ES(t)$. The time dependence of $S^*(t) + S(t) = [S(t)]$ and $P^*(t) +$



671 $P(t) = [P(t)]$ are shown in Fig. 7(b), right panel, and $ES^*(t) + ES(t) = [ES(t)]$ and $[E(t)]$ are shown in Fig.
 672 7(c), right panel, which recapture conventional chemical kinetics of $[S(t)]$, $[ES(t)]$, $[P(t)]$ and $[E(t)]$, as required
 673 for mathematical and physical consistency.

674

675

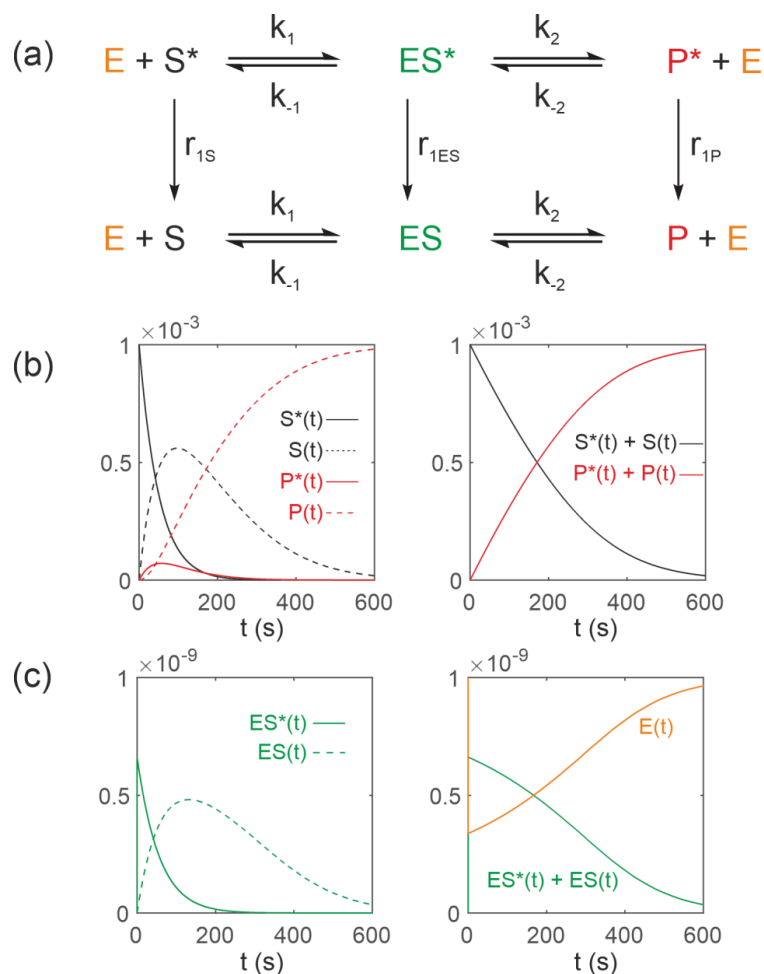


Figure 7 Simulated Michaelis-Menten kinetics for exchange of hyperpolarized solutes $E + S^* \leftrightarrow ES^* \leftrightarrow P^* + E$ conforming to conservation of mass, assuming initial hyperpolarized magnetization of only solute $S^*(0) = 0.001$ and $[E]_0 = 1 \times 10^{-9}$ M. Longitudinal relaxation rate constants were $R_{1S} = R_{1ES} = R_{1P} = 1/60s^{-1}$. The reaction rate constants were $k_1 = 1 \times 10^7 s^{-1}$, $k_{-1} = 1 \times 10^2 s^{-1}$, $k_2 = 5 \times 10^3 s^{-1}$ and $k_{-2} = 0 s^{-1}$, such that $K_M = 5.1 \times 10^{-4} M$ and $V_{max} = 5 \times 10^{-6} M s^{-1}$. Left panels: (b) Simulated time dependence of $S^*(t)$, $S(t)$, $P^*(t)$ and $P(t)$; and (c) simulated time dependence of $ES^*(t)$ and $ES(t)$. Right panels: (b) simulated time dependence of $S^*(t) + S(t) = [S(t)]$ and $P^*(t) + P(t) = [P(t)]$; and (c) $ES^*(t) + ES(t) = [ES(t)]$ and $[E(t)]$.



676 It is worth considering some of the consequences of Eq. (66) when studying enzyme mediated reactions
 677 with hyperpolarized substrates. When the substrate concentration $[S^*(t) + S(t)]$ is much greater than K_M then the
 678 rate of product formation $d([P^*(t) + P(t)])/dt$ is given by $v = k_2[E]_0 = V_{max}$, which is constant (*i.e.*, it is
 679 effectively a zero order reaction with respect to substrate concentration). The enzyme is said to be saturated; its
 680 rate is independent of substrate concentration but V_{max} is proportional to the enzyme concentration $[E]_0$. When
 681 the substrate concentration $[S^*(t) + S(t)]$ is much less than K_M then the rate of product formation
 682 $d([P^*(t) + P(t)])/dt$ is given by $V = k_2[E]_0[S^*(t) + S(t)]/K_M$ and the reaction is effectively first order with
 683 respect to substrate concentration. Nevertheless, the rate is still proportional to $[E]_0$. The kinetics of enzyme
 684 systems, and indeed enzyme kinetics in general, are a composite of the two parameters K_M and V_{max} . The influences
 685 on one cannot be distinguished from the other on the basis of time-course experiments alone; separate
 686 measurements that are needed to estimate the total enzyme concentration.

687 Further simulations were performed to explore the influence of a much shorter value of T_1^{ES} for the
 688 enzyme substrate complex, while T_1^S and T_1^P were unchanged. Even if it were assumed to be very small *viz.*,
 689 $T_1^{ES} = 276.4$ ms the time evolution was indistinguishable from that presented in Fig. 7; the corresponding curves
 690 were superimposable. The signal that resided on the enzyme substrate complex ES^* was 6 orders of magnitude
 691 lower than that of the substrate S^* and product P^* . Therefore, the kinetics of signal evolution were dominated by
 692 T_1^S and T_1^P while changes in T_1^{ES} could be ignored. An exception to this analysis might occur if the active site were
 693 next to a paramagnetic centre, such as is found in metalloproteins for which T_1^{ES} could be very much shorter than
 694 predicted (see the relaxation theory section above).

695

696 5.3 Enzyme inhibition and hyperpolarized substrate kinetics

697 Our formalism can be readily extended to account for the influence of a ligand/solute to inhibit an
 698 enzyme. The simplest case is when a solute binds reversibly to the free enzyme E to form an enzyme inhibitor
 699 complex EI; hence, the enzyme becomes unable to bind and react with its substrate S. To describe this scenario,
 700 Eq. 45 is modified to include an additional pathway for the loss of free enzyme:

701

$$\frac{d[E(t)]}{dt} = -k_1[E(t)][S^*(t) + S(t)] + (k_{-1} + k_2)[ES^*(t) + ES(t)] - k_{-2}[E(t)][P^*(t) + P(t)] - k_3[E(t)][I(t)] + k_{-3}[EI(t)] \quad (67)$$

702

703 The model is now extended to include differential equations describing the concentration of the inhibitor $[I(t)]$
 704 and the enzyme-inhibitor complex $[EI(t)]$:

705

$$\frac{d[I(t)]}{dt} = -k_3[E(t)][I(t)] + k_{-3}[EI(t)] \quad (68)$$

$$\frac{d[EI(t)]}{dt} = k_3[E(t)][I(t)] - k_{-3}[EI(t)] \quad (69)$$

706 Such equations can be incorporated into the Michaelis-Menten equations and we develop this next.



707 5.3.1 Types of enzyme inhibition

708 There are three commonly encountered types of reversible enzyme inhibition (Kuchel, 2009): (i) a *competitive*
709 inhibitor is structurally similar to the substrate and binds preferentially in the active site of the free enzyme, E,
710 thus preventing the substrate from binding and reacting; (ii) an *uncompetitive* inhibitor binds only to the enzyme-
711 substrate complex and therefore causes substrate-concentration dependent inhibition; and (iii), a *non-competitive*
712 inhibitor binds to both the free enzyme and to the enzyme-substrate complex; it causes a conformational change
713 at the active site that inhibits (or even enhances) the reaction. Such an effect is referred to as allosteric inhibition
714 (or activation).

715 Accounting for all three scenarios, the free enzyme concentration is given by:

716

$$[E(t)] = [E]_0 - [EI(t)] - [ES^*(t) + ES(t)] - [ESI^*(t) + ESI(t)] \quad (70)$$

717

718 Substituting:

719

$$\alpha = 1 + \frac{[I(t)]}{K_I} \quad \text{and} \quad \alpha' = 1 + \frac{[I(t)]}{K_I'} \quad , \quad (71)$$

720

721 where $K_I = [E(t)][I(t)]/[EI(t)]$ and $K_I' = [ES(t)][I(t)]/[ESI(t)]$, yields:

722

$$\frac{d([P^*(t) + P(t)])}{dt} = \frac{k_2[E]_0[S^*(t) + S(t)]}{\alpha K_M + \alpha'[S^*(t) + S(t)]} \quad (72)$$

723

724 The three types of enzyme inhibition can be distinguished by their influence on the kinetic parameters that are
725 estimated in specially designed experiments performed on the enzyme over a range of substrate and inhibitor
726 concentrations (Kuchel, 2009): (i) competitive inhibitors cause an increase in apparent K_M value while V_{max} is
727 unchanged; (ii) uncompetitive inhibitors cause a reduction in V_{max} while the apparent K_M is unchanged; and (iii)
728 non-competitive inhibitors cause both a reduction in V_{max} and an increase in apparent K_M .

729 An additional effect that can be considered is where either the substrate of the reaction $[S(t)]$, or the
730 product of the reaction, $[P(t)]$, acts as the inhibitor, called unsurprisingly ‘substrate inhibition’ and ‘product
731 inhibition’, respectively. The relevant enzyme kinetic equations are composed by substituting $[I(t)] =$
732 $[S^*(t) + S(t)]$ or $[I(t)] = [P^*(t) + P(t)]$ in the above equations (refs).

733

734 6 Cofactors and unlabelled pools – Lactate Dehydrogenase

735 We now consider a real system that is of contemporary interest for *in vivo* clinical studies using dDNP.
736 It is lactate dehydrogenase (E.C. 1.1.1.27). Consider the LDH catalysed reaction of a hyperpolarized substrate; it
737 follows an ordered sequential reaction in which $E + NADH \leftrightarrow E \cdot NADH + Pyr^* \leftrightarrow E \cdot NAD + Lac^* \leftrightarrow E + NAD^+$.
738 Again, we assume that relaxation of magnetization occurs through T_1 processes to form a pool of reactants E +



739 NADH \leftrightarrow E·NADH + Pyr \leftrightarrow E·NAD + Lac \leftrightarrow E + NAD⁺ as shown in Fig. 8(a). The relevant differential
 740 equations used to describe the kinetics are (omitting the square brackets that denote concentration):
 741

$$\frac{dPyr^*(t)}{dt} = -k_2 E \cdot NADH(t) Pyr^*(t) + k_{-2} E \cdot NAD(t) Lac^*(t) - R_1^P Pyr^*(t) \quad , \quad (73)$$

$$\frac{dPyr(t)}{dt} = -k_2 E \cdot NADH(t) Pyr(t) + k_{-2} E \cdot NAD(t) Lac(t) + R_1^P Pyr^*(t) \quad , \quad (74)$$

$$\frac{dLac^*(t)}{dt} = k_2 E \cdot NADH(t) Pyr^*(t) - k_{-2} E \cdot NAD(t) Lac^*(t) - R_1^L Lac^*(t) \quad , \quad (75)$$

$$\frac{dLac(t)}{dt} = k_2 E \cdot NADH(t) Pyr(t) - k_{-2} E \cdot NAD(t) Lac(t) + R_1^L Lac^*(t) \quad , \quad (76)$$

$$\frac{dNADH(t)}{dt} = -k_1 E(t) NADH(t) + k_{-1} E \cdot NADH(t) \quad , \quad (77)$$

$$\frac{dNAD(t)}{dt} = k_3 E \cdot NAD(t) - k_{-3} E(t) NAD(t) \quad , \quad (78)$$

$$\begin{aligned} \frac{dE \cdot NADH(t)}{dt} &= k_1 E(t) NADH(t) - k_{-1} E \cdot NADH(t) - k_2 E \cdot NADH(t) (Pyr^*(t) + Pyr(t)) \\ &\quad + k_{-2} E \cdot NAD(t) (Lac^*(t) + Lac(t)) \quad , \end{aligned} \quad (79)$$

$$\begin{aligned} \frac{dE \cdot NAD(t)}{dt} &= k_2 E \cdot NADH(t) (Pyr^*(t) + Pyr(t)) - k_{-2} E \cdot NAD(t) (Lac^*(t) + Lac(t)) \\ &\quad - k_3 E \cdot NAD(t) + k_{-3} E(t) NAD(t) \quad , \end{aligned} \quad (80)$$

$$\frac{dE(t)}{dt} = -k_1 E(t) NADH(t) + k_{-1} E \cdot NADH(t) + k_3 E \cdot NAD(t) - k_{-3} E(t) NAD(t) \quad , \quad (81)$$

742

743 where $E(t)$ is the concentration of free enzyme, $NAD(t)$ and $NADH(t)$ are the concentrations of the free co-
 744 factors, $E \cdot NAD(t)$ and $E \cdot NADH(t)$ are the concentrations of the enzyme-cofactor complexes and $Pyr(t)$ and
 745 $Lac(t)$ are the free substrates with relaxation rate constants R_1^P and R_1^L , respectively.

746 Mass is conserved as is confirmed by the fact that $d(Pyr^*(t) + Pyr(t) + Lac^*(t) + Lac(t))/dt = 0$.
 747 Enzyme concentration is conserved as is confirmed by $d(E \cdot NADH(t) + E \cdot NAD(t) + E(t))/dt = 0$ and
 748 cofactor pools are conserved as is confirmed by $d(NADH(t) + NAD(t) + E \cdot NADH(t) + E \cdot NAD(t))/dt = 0$.
 749 Therefore, provided $Pyr^*(0) + Pyr(0) = [Pyr]_0$ and $Lac^*(0) + Lac(0) = [Lac]_0$ then $Pyr^*(t) + Pyr(t) =$
 750 $[Pyr(t)]$ and $Lac^*(t) + Lac(t) = [Lac(t)]$, respectively.

751 Figure 8(b) shows numerical simulations of the time evolution of the system that is described by Eqs.
 752 (73-81) with initial hyperpolarized signal/concentration (see above for a comment on this aspect) $Pyr^*(t) =$
 753 0.001 and longitudinal relaxation rate constants $R_1^P = R_1^L = 1/60s^{-1}$. The kinetic parameters used for lactate
 754 dehydrogenase were as previously published (Witney et al., 2011; Zewe and Fromm, 1962) for the rabbit muscle
 755 enzyme. Enzyme concentration was $[E]_0 = 1.2 \times 10^{-9}$ M and rate constants $k_1 = 1.03 \times 10^8 s^{-1}$, $k_{-1} =$
 756 $549 s^{-1}$, $k_2 = 6.72 \times 10^6 s^{-1}$, $k_{-2} = 3.44 \times 10^4 s^{-1}$, $k_3 = 842 s^{-1}$, and $k_{-3} = 9.12 \times 10^5 s^{-1}$. Initial



757 cofactor concentrations were $[NADH(0)] = 1.0 \times 10^{-4}$ M and $[NAD(0)] = 1.0 \times 10^{-3}$ M to give a $[NAD]/$
 758 $[NADH]$ ratio of 10. In the first instance, endogenous pools of hyperpolarized lactate were set to $Lac^*(0) = 0$,
 759 and unpolarized pools of both pyruvate and lactate were made zero, *viz.*, $Pyr(0) = 0$ and $Lac(0) = 0$.

760

761

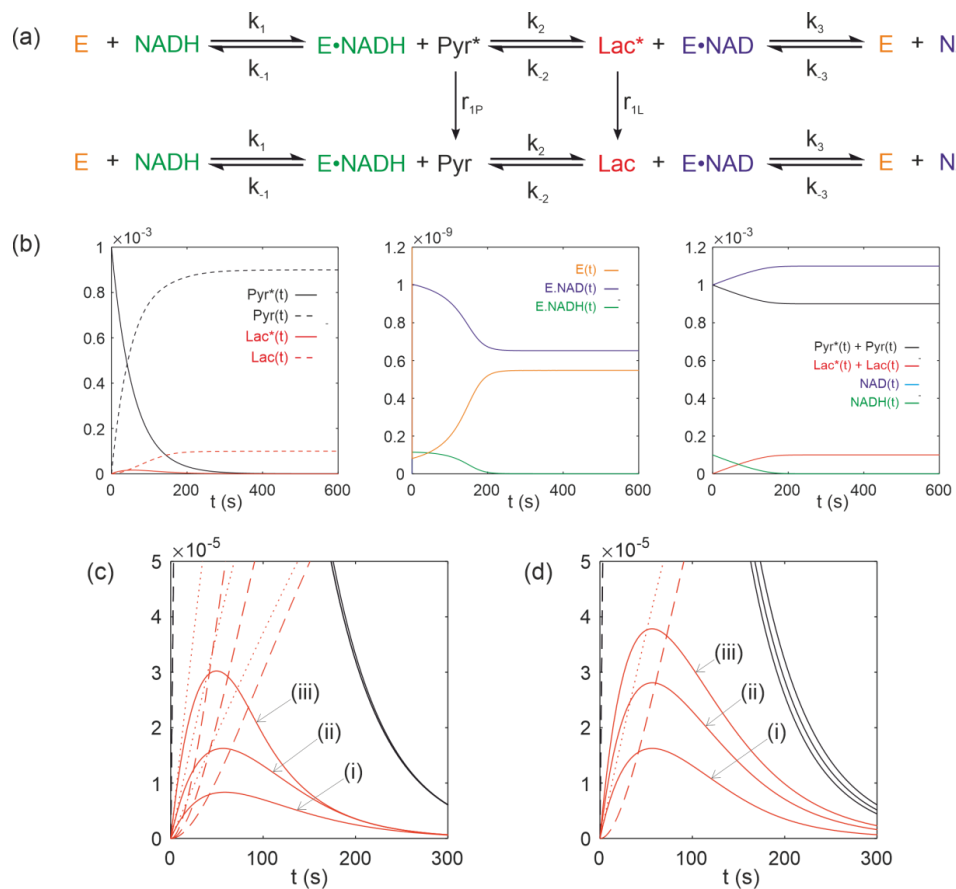


Figure 8 Simulated kinetics of lactate dehydrogenase for exchange of solutes, $E + NADH \leftrightarrow E \cdot NADH + Pyr^* \leftrightarrow E \cdot NAD + Lac^* \leftrightarrow E + NAD^+$, conforming to conservation of mass, assuming initial hyperpolarized magnetization of only solute $Pyr^*(0) = 0.001$ and $[E]_0 = 1.2 \times 10^{-9}$ M. Longitudinal relaxation rate constants were $R_1^P = R_1^L = 1/60s^{-1}$. Rate constants were $k_1 = 1.03 \times 10^8 s^{-1}$, $k_{-1} = 549 s^{-1}$, $k_2 = 6.72 \times 10^6 s^{-1}$, $k_{-2} = 3.44 \times 10^4 s^{-1}$, $k_3 = 842 s^{-1}$ and $k_{-3} = 9.12 \times 10^5 s^{-1}$. Initial cofactor concentrations were $[NADH(0)] = 1.0 \times 10^{-4}$ M and $[NAD(0)] = 1.0 \times 10^{-3}$ M. (b) Simulated time dependence $Pyr^*(t)$, $Pyr(t)$, $Lac^*(t)$ and $Lac(t)$ left panel, $[E(t)]$, $[E \cdot NAD(t)]$ and $[E \cdot NADH(t)]$, middle panel, and $Pyr^*(t) + Pyr(t) = [Pyr(t)]$, $Lac^*(t) + Lac(t) = [Lac(t)]$, $[NAD(t)]$ and $[NADH(t)]$, right panel. (c) Simulations of the time dependence of $Lac^*(t)$ under the conditions that: $[E]_0 = (i) 0.6 \times 10^{-9}$ M; (ii) 1.2×10^{-9} M; and (iii) 2.4×10^{-9} M, while all other parameters remained unchanged. (d) Simulations of the time dependence of $Lac^*(t)$ under the conditions that: $Lac(0) = (i) 0$ mM; (ii) 20 mM; and (iii) 40 mM, while all other parameters remained unchanged.



762 The computed time dependence of polarized and unpolarized pools $Pyr^*(t)$, $Pyr(t)$, $Lac^*(t)$ and
763 $Lac(t)$ are shown in Fig. 8(b), left panel. The time dependence of $[E(t)]$, $[E.NAD(t)]$ and $[E.NADH(t)]$ are
764 shown in Fig. 8(b), middle panel. The time dependence of $Pyr^*(t) + Pyr(t) = [Pyr(t)]$, $Lac^*(t) + Lac(t) =$
765 $[Lac(t)]$, $[NAD(t)]$ and $[NADH(t)]$ are shown in Fig. 8(b), right panel. Several interesting features are evident.
766 First, the model predicted the expected time dependences of both hyperpolarized pyruvate $Pyr^*(t)$ and its
767 conversion to $Lac^*(t)$. Under the conditions of the simulation, the free enzyme $[E(t)]$ was rapidly depleted to
768 form an equilibrium of $[E.NAD(t)]$ and $[E.NADH(t)]$. During the reaction with $Pyr^*(t)$, the equilibrium
769 position of the enzyme was altered to give a final equilibrium position that could then be appreciated from the
770 total pools of $Pyr^*(t) + Pyr(t) = [Pyr(t)]$ and $Lac^*(t) + Lac(t) = [Lac(t)]$, which predicts a net conversion
771 of $[Pyr(t)]$ to $[Lac(t)]$ of ~10%.

772 Finally, we consider real case scenarios that are reported in the literature. Figure 8(c) shows the situation
773 where the LDH expression level is altered by the progression of disease (LDH expression is known to be
774 upregulated in more aggressive cancer phenotypes (Albers et al., 2008)) or down regulated during therapy (Ward
775 et al., 2010), which can be explored through the value of $[E]_0$. Figure 8(c) shows simulations of the $Lac^*(t)$ signal
776 under the condition that: $[E]_0 = (i) 0.6 \times 10^{-9}$ M; $(ii) 1.2 \times 10^{-9}$ M; and $(iii) 2.4 \times 10^{-9}$ M, while all other
777 parameters remained unchanged, relative to those used for Fig. 8(b). It is apparent that increased enzyme
778 expression leads to an increase in the apparent rate of conversion of $Pyr^*(t)$ to $Lac^*(t)$ even in the absence of a
779 change in enzyme activity, as seen in real experiments. Another situation that is frequently encountered are
780 changes in the pool size of endogenous lactate, for example in response to hypoxia, which can be explored through
781 the parameter $Lac(0)$. Figure 8(d) shows simulations of the $Lac^*(t)$ signal under the conditions that: $Lac(0) =$
782 $(i) 0$ mM; $(ii) 20$ mM; and $(iii) 40$ mM, while all other parameters remained unchanged, relative to those used to
783 generate Fig. 8(b). The model therefore predicts that an increased pool of endogenous unpolarized lactate leads to
784 an increase in the apparent rate of conversion of $Pyr^*(t)$ to $Lac^*(t)$, as reported widely in the literature (Day et
785 al., 2007).

786

787 **7 Conclusion**

788 We have described an approach to formulating the kinetic master equations that describe the time evolution of
789 hyperpolarized ^{13}C NMR signals in reacting (bio)chemical systems, including enzymes with two or more
790 substrates, and various enzyme reaction mechanisms as classified by Cleland. The modelling can be the basis of
791 simulating many pertinent features that are seen in dDNP experiments. Derivation of the Michaelis-Menten
792 equation in the context of dDNP experiments illustrates why formation of a hyperpolarized enzyme-substrate
793 complex does *not* cause an appreciable loss of the signal from the substrate or product. It was also able to answer
794 why the concentration of an unlabelled pool of substrate, for example ^{12}C lactate, causes an increase in the rate of
795 exchange of the ^{13}C labelled pool, and to what extent the equilibrium position of an enzyme-catalyzed reaction,
796 for example LDH, is altered upon adding hyperpolarized substrate. The formalism described here should
797 contribute to a fuller mechanistic understanding of the time courses derived from dDNP experiments and will be
798 relevant to ongoing clinical applications using dDNP.

799

800



801 **Author contributions**

802 All authors planned the research, conducted the research and wrote the paper.

803

804 **Competing interests**

805 The authors declare that they have no conflict of interest.

806

807 **Acknowledgements**

808 The work was supported by the NIHR Biomedical Research Centre at Guy's and St Thomas' NHS Foundation
809 Trust and KCL; the Centre of Excellence in Medical Engineering funded by the Wellcome Trust and EPSRC (WT
810 203148/Z/16/Z) and the BHF Centre of Research Excellence (RE/18/2/34213). PWK's work was supported by
811 and Australian Research Council Discovery Project Grant, DP190100510. SJE was supported by ENS-Lyon, the
812 French CNRS, Lyon 1 University and the European Research Council under the European Union's Horizon 2020
813 research and innovation program (ERC Grant Agreements No. 714519 / HP4all).

814

815



816

References

817

- 818 Albers, M. J., Bok, R., Chen, A. P., Cunningham, C. H., Zierhut, M. L., Zhang, V. Y., Kohler, S. J., Tropp, J.,
819 Hurd, R. E., Yen, Y. F., Nelson, S. J., Vigneron, D. B., and Kurhanewicz, J.: Hyperpolarized C-13 Lactate,
820 Pyruvate, and Alanine: Noninvasive Biomarkers for Prostate Cancer Detection and Grading, *Cancer Res.*, 68,
821 8607-8615, doi:10.1158/0008-5472.Can-08-0749, 2008.
- 822 Allard, P., Helgstrand, M., and Hard, T.: The complete homogeneous master equation for a heteronuclear two-
823 spin system in the basis of cartesian product operators, *J. Magn. Reson.*, 134, 7-16, doi:10.1006/jmre.1998.1509,
824 1998.
- 825 Ardenkjaer-Larsen, J. H., Fridlund, B., Gram, A., Hansson, G., Hansson, L., Lerche, M. H., Servin, R., Thaning,
826 M., and Golman, K.: Increase in signal-to-noise ratio of > 10,000 times in liquid-state NMR, *Proc. Natl. Acad.*
827 *Sci. U. S. A.*, 100, 10158-10163, doi:10.1073/pnas.1733835100, 2003.
- 828 Ardenkjaer-Larsen, J. H., Boebinger, G. S., Comment, A., Duckett, S., Edison, A. S., Engelke, F., Griesinger,
829 C., Griffin, R. G., Hilty, C., Maeda, H., Parigi, G., Prisner, T., Ravera, E., van Bentum, J., Vega, S., Webb, A.,
830 Luchinat, C., Schwalbe, H., and Frydman, L.: Facing and Overcoming Sensitivity Challenges in Biomolecular
831 NMR Spectroscopy, *Angew. Chem. Int. Ed. Engl.*, 54, 9162-9185, doi:10.1002/anie.201410653, 2015.
- 832 Bechmann, M., Dusold, S., Sebald, A., Shuttleworth, W. A., Jakeman, D. L., Mitchell, D. J., and Evans, J. N. S.:
833 ¹³C chemical shielding tensor orientations in a phosphoenolpyruvate moiety from ¹³C rotational-resonance
834 MAS NMR lineshapes, *Solid State Sci.*, 6, 1097-1105, doi.org/10.1016/j.solidstatesciences.2004.04.021, 2004.
- 835 Bengs, C., and Levitt, M. H.: A master equation for spin systems far from equilibrium, *J. Magn. Reson.*, 310,
836 106645, doi:10.1016/j.jmr.2019.106645, 2020.
- 837 Blumberg, W. E.: Nuclear Spin-Lattice Relaxation Caused by Paramagnetic Impurities, *Phys. Rev.*, 119, 79-84,
838 doi.org/10.1103/PhysRev.119.79, 1960.
- 839 Chiavazza, E., Kubala, E., Gringeri, C. V., Duwel, S., Durst, M., Schulte, R. F., and Menzel, M. I.: Earth's
840 magnetic field enabled scalar coupling relaxation of ¹³C nuclei bound to fast-relaxing quadrupolar ¹⁴N in
841 amide groups, *J. Magn. Reson.*, 227, 35-38, doi:10.1016/j.jmr.2012.11.016, 2013.
- 842 Cleland, W. W.: Enzyme kinetics, *Annu. Rev. Biochem.*, 36, 77-112,
843 doi:10.1146/annurev.bi.36.070167.000453, 1967.
- 844 Comment, A., and Merritt, M. E.: Hyperpolarized Magnetic Resonance as a Sensitive Detector of Metabolic
845 Function, *Biochemistry*, 53, 7333-7357, doi:10.1021/bi501225t, 2014.
- 846 Cook, P. F., and Cleland, W. W.: Enzyme Kinetics and Mechanism, Taylor & Francis Group, New York, 2007.
- 847 Daniels, C. J., McLean, M. A., Schulte, R. F., Robb, F. J., Gill, A. B., McGlashan, N., Graves, M. J., Schwaiger,
848 M., Lomas, D. J., Brindle, K. M., and Gallagher, F. A.: A comparison of quantitative methods for clinical
849 imaging with hyperpolarized (¹³C)-pyruvate, *NMR Biomed.*, 29, 387-399, 10.1002/nbm.3468, 2016.
- 850 Day, S. E., Kettunen, M. I., Gallagher, F. A., Hu, D. E., Lerche, M., Wolber, J., Golman, K., Ardenkjaer-Larsen,
851 J. H., and Brindle, K. M.: Detecting tumor response to treatment using hyperpolarized ¹³C magnetic resonance
852 imaging and spectroscopy, *Nat. Med.*, 13, 1382-1387, doi:10.1038/nm1650, 2007.
- 853 Elliott, S. J., Bengs, C., Brown, L. J., Hill-Cousins, J. T., O'Leary, D. J., Pileio, G., and Levitt, M. H.: Nuclear
854 singlet relaxation by scalar relaxation of the second kind in the slow-fluctuation regime, *J. Chem. Phys.*, 150,
855 064315, 10.1063/1.5074199, 2019.



- 856 Endre, Z. H., Chapman, B. E., and Kuchel, P. W.: Intra-Erythrocyte Microviscosity and Diffusion of
857 Specifically Labeled [Glycyl-Alpha-C-13]Glutathione by Using C-13 Nmr, *Biochem. J.*, 216, 655-660,
858 doi:10.1042/bj2160655, 1983.
- 859 Ernst, R. R., Bodenhausen, G., and Wokaun, A.: Principles of Nuclear Magnetic Resonance in One and Two
860 Dimensions, Clarendon Press, Oxford, 1987.
- 861 Gabellieri, C., Reynolds, S., Lavie, A., Payne, G. S., Leach, M. O., and Eykyn, T. R.: Therapeutic target
862 metabolism observed using hyperpolarized N-15 choline, *J. Am. Chem. Soc.*, 130, 4598-4599,
863 doi:10.1021/ja8001293, 2008.
- 864 Golman, K., Ardenkjaer-Larsen, J. H., Petersson, J. S., Mansson, S., and Leunbach, I.: Molecular imaging with
865 endogenous substances, *Proc. Natl. Acad. Sci. U. S. A.*, 100, 10435-10439, doi:10.1073/pnas.1733836100,
866 2003.
- 867 Golman, K., in't Zandt, R., Lerche, M., Pehrson, R., and Ardenkjaer-Larsen, J. H.: Metabolic imaging by
868 hyperpolarized ¹³C magnetic resonance imaging for in vivo tumor diagnosis, *Cancer Res.*, 66, 10855-10860,
869 doi:10.1158/0008-5472.CAN-06-2564, 2006.
- 870 Helgstrand, M., Hard, T., and Allard, P.: Simulations of NMR pulse sequences during equilibrium and non-
871 equilibrium chemical exchange, *J. Biomol. NMR*, 18, 49-63, doi:10.1023/a:1008309220156, 2000.
- 872 Hill, D. K., Jamin, Y., Orton, M. R., Tardif, N., Parkes, H. G., Robinson, S. P., Leach, M. O., Chung, Y. L., and
873 Eykyn, T. R.: H-1 NMR and hyperpolarized C-13 NMR assays of pyruvate-lactate: a comparative study, *NMR*
874 *Biomed.*, 26, 1321-1325, 10.1002/nbm.2957, 2013a.
- 875 Hill, D. K., Orton, M. R., Mariotti, E., Boulton, J. K., Panek, R., Jafar, M., Parkes, H. G., Jamin, Y., Miniotis, M.
876 F., Al-Saffar, N. M., Belouche-Babari, M., Robinson, S. P., Leach, M. O., Chung, Y. L., and Eykyn, T. R.:
877 Model free approach to kinetic analysis of real-time hyperpolarized ¹³C magnetic resonance spectroscopy data,
878 *Plos One*, 8, e71996, doi:10.1371/journal.pone.0071996, 2013b.
- 879 Hore, P. J., Jones, J., and Wimperis, S.: NMR: The Toolkit, Second Edition ed., Oxford Chemistry Primers,
880 Oxford University Press, 2015.
- 881 Hu, S., Lustig, M., Balakrishnan, A., Larson, P. E. Z., Bok, R., Kurhanewicz, J., Nelson, S. J., Goga, A., Pauly,
882 J. M., and Vigneron, D. B.: 3D Compressed Sensing for Highly Accelerated Hyperpolarized C-13 MRSI With
883 In Vivo Applications to Transgenic Mouse Models of Cancer, *Magn. Reson. Med.*, 63, 312-321,
884 10.1002/mrm.22233, 2010.
- 885 Johnson, J.: Thermal agitation of electricity in conductors, *Phys. Rev.*, 32, 97-109, doi:10.1103/physrev.32.97,
886 1928.
- 887 Keeler, J.: Understanding NMR spectroscopy, Second Edition ed., John Wiley & Sons, Ltd, 2010.
- 888 Keshari, K. R., and Wilson, D. M.: Chemistry and biochemistry of C-13 hyperpolarized magnetic resonance
889 using dynamic nuclear polarization, *Chem. Soc. Rev.*, 43, 1627-1659, doi:10.1039/C3cs60124b, 2014.
- 890 Kowalewski, J., and Maler, L.: Nuclear spin relaxation in liquids: theory, experiments and applications, 2nd
891 Edition ed., CRC Press, Taylor & Francis, Boca Raton, FL, 2019.
- 892 Kubica, D., Wodynski, A., Kraska-Dziadecka, A., and Gryff-Keller, A.: Scalar relaxation of the second kind. A
893 potential source of information on the dynamics of molecular movements. 3. A (¹³C) nuclear spin relaxation
894 study of CBrX₃ (X = Cl, CH₃, Br) molecules, *J Phys Chem A*, 118, 2995-3003, doi:10.1021/jp501064c, 2014.
- 895 Kuchel, P. W.: Schaum's Outline of Biochemistry, 3rd Edition ed., McGraw-Hill Companies, Inc, 2009.



- 896 Kuchel, P. W., Karlsson, M., Lerche, M. H., Shishmarev, D., and Ardenkjaer-Larsen, J. H.: Rapid zero-trans
897 kinetics of Cs⁺ exchange in human erythrocytes quantified by dissolution hyperpolarized Cs-133(+) NMR
898 spectroscopy, *Sci. Rep.*, 9, 19726, doi:10.1038/s41598-019-56250-z, 2019.
- 899 Kuchel, P. W., and Shishmarev, D.: Dissolution dynamic nuclear polarization NMR studies of enzyme kinetics:
900 Setting up differential equations for fitting to spectral time courses, *J. Magn. Reson. Open*, 1, 100001,
901 doi.org/10.1016/j.jmro.2020.100001, 2020.
- 902 Kuhne, R. O., Schaffhauser, T., Wokaun, A., and Ernst, R. R.: Study of Transient-Chemical Reactions by Nmr -
903 Fast Stopped-Flow Fourier-Transform Experiments, *J. Magn. Reson.*, 35, 39-67, doi:10.1016/0022-
904 2364(79)90077-5, 1979.
- 905 Levitt, M. H., and Dibri, L.: Steady-State in Magnetic-Resonance Pulse Experiments, *Phys. Rev. Lett.*, 69,
906 3124-3127, DOI 10.1103/PhysRevLett.69.3124, 1992.
- 907 Mariotti, E., Orton, M. R., Eerbeek, O., Ashruf, J. F., Zuurbier, C. J., Southworth, R., and Eykyn, T. R.:
908 Modeling non-linear kinetics of hyperpolarized [1-C-13] pyruvate in the crystalloid-perfused rat heart, *NMR*
909 *Biomed.*, 29, 377-386, 10.1002/nbm.3464, 2016.
- 910 Matson, G. B.: Methyl NMR relaxation: The effects of spin rotation and chemical shift anisotropy mechanisms,
911 *J. Chem. Phys.*, 67, 5152-5161, doi.org/10.1063/1.434744, 1977.
- 912 McConnell, H. M.: Reaction Rates by Nuclear Magnetic Resonance, *J. Chem. Phys.*, 28, 430-431,
913 doi:10.1063/1.1744152, 1958.
- 914 Mieville, P., Ahuja, P., Sarkar, R., Jannin, S., Vasos, P. R., Gerber-Lemaire, S., Mishkovsky, M., Comment, A.,
915 Gruetter, R., Ouari, O., Tordo, P., and Bodenhausen, G.: Scavenging Free Radicals To Preserve Enhancement
916 and Extend Relaxation Times in NMR using Dynamic Nuclear Polarization, *Angew. Chem. Int. Ed. Engl.*, 49,
917 6182-6185, doi:10.1002/anie.201000934, 2010.
- 918 Milani, J., Vuichoud, B., Bornet, A., Mieville, P., Mottier, R., Jannin, S., and Bodenhausen, G.: A magnetic
919 tunnel to shelter hyperpolarized fluids, *Rev. Sci. Instrum.*, 86, 024101, doi:10.1063/1.4908196, 2015.
- 920 Pages, G., Puckeridge, M., Guo, L. F., Tan, Y. L., Jacob, C., Garland, M., and Kuchel, P. W.: Transmembrane
921 Exchange of Hyperpolarized C-13-Urea in Human Erythrocytes: Subminute Timescale Kinetic Analysis,
922 *Biophys. J.*, 105, 1956-1966, doi:10.1016/j.bpj.2013.09.034, 2013.
- 923 Pagès, G., and Kuchel, P. W.: FmR alpha analysis: Rapid and direct estimation of relaxation and kinetic
924 parameters from dynamic nuclear polarization time courses, *Magn. Reson. Med.*, 73, 2075-2080,
925 doi:10.1002/mrm.25345, 2015.
- 926 Pell, A. J., Pintacuda, G., and Grey, C. P.: Paramagnetic NMR in solution and the solid state, *Prog. Nucl. Magn.*
927 *Reson. Spectrosc.*, 111, 1-271, doi:10.1016/j.pnmrs.2018.05.001, 2019.
- 928 Pileio, G.: Singlet state relaxation via scalar coupling of the second kind, *J. Chem. Phys.*, 135, 174502,
929 doi:10.1063/1.3651479, 2011.
- 930 Shishmarev, D., Kuchel, P. W., Pagès, G., Wright, A. J., Hesketh, R. L., Kreis, F., and Brindle, K. M.:
931 Glyoxalase activity in human erythrocytes and mouse lymphoma, liver and brain probed with hyperpolarized C-
932 13-methylglyoxal, *Commun. Biol.*, 1, 232, doi:10.1038/s42003-018-0241-1, 2018a.
- 933 Shishmarev, D., Wright, A. J., Rodrigues, T. B., Pileio, G., Stevanato, G., Brindle, K. M., and Kuchel, P. W.:
934 Sub-minute kinetics of human red cell fumarase: H-1 spin-echo NMR spectroscopy and C-13 rapid-dissolution
935 dynamic nuclear polarization, *NMR Biomed.*, 31, e3870, doi:10.1002/nbm.3870, 2018b.



- 936 Valensin, G., Kushnir, T., and Navon, G.: Selective and Non-Selective Proton Spin-Lattice Relaxation Studies
937 of Enzyme-Substrate Interactions, *J. Magn. Reson.*, 46, 23-29, doi:10.1016/0022-2364(82)90159-7, 1982.
- 938 van Heeswijk, R. B., Uffmann, K., Comment, A., Kurdzesau, F., Perazzolo, C., Cudalbu, C., Jannin, S., Konter,
939 J. A., Hautle, P., van den Brandt, B., Navon, G., van der Klink, J. J., and Gruetter, R.: Hyperpolarized lithium-6
940 as a sensor of nanomolar contrast agents, *Magn. Reson. Med.*, 61, 1489-1493, doi:10.1002/mrm.21952, 2009.
- 941 Ward, C. S., Venkatesh, H. S., Chaumeil, M. M., Brandes, A. H., VanCrickinge, M., Dafni, H., Sukumar, S.,
942 Nelson, S. J., Vigneron, D. B., Kurhanewicz, J., James, C. D., Haas-Kogan, D. A., and Ronen, S. M.:
943 Noninvasive Detection of Target Modulation following Phosphatidylinositol 3-Kinase Inhibition Using
944 Hyperpolarized C-13 Magnetic Resonance Spectroscopy, *Cancer Res.*, 70, 1296-1305, doi:10.1158/0008-
945 5472.Can-09-2251, 2010.
- 946 Weber, E. M. M., Kurzbach, D., and Abergel, D.: A DNP-hyperpolarized solid-state water NMR MASER:
947 observation and qualitative analysis, *Phys. Chem. Chem. Phys.*, 21, 21278-21286, doi:10.1039/c9cp03334c,
948 2019.
- 949 Wilbur, D. J., Norton, R. S., Clouse, A. O., Addleman, R., and Allerhand, A.: Determination of rotational
950 correlation times of proteins in solution from carbon-13 spin-lattice relaxation measurements. Effect of
951 magnetic field strength and anisotropic rotation, *J. Am. Chem. Soc.*, 98, 8250-8254, doi:10.1021/ja00441a059,
952 1976.
- 953 Witney, T. H., Kettunen, M. I., and Brindle, K. M.: Kinetic modeling of hyperpolarized ¹³C label exchange
954 between pyruvate and lactate in tumor cells, *J. Biol. Chem.*, 286, 24572-24580, doi:10.1074/jbc.M111.237727,
955 2011.
- 956 Wolber, J., Ellner, F., Fridlund, B., Gram, A., Johannesson, H., Hansson, G., Hansson, L. H., Lerche, M. H.,
957 Mansson, S., Servin, R., Thaning, M., Golman, K., and Ardenkjaer-Larsen, J. H.: Generating highly polarized
958 nuclear spins in solution using dynamic nuclear polarization, *Nucl. Instrum. Meth. A*, 526, 173-181,
959 doi:10.1016/j.nima.2004.03.171, 2004.
- 960 Yen, Y. F., Kohler, S. J., Chen, A. P., Tropp, J., Bok, R., Wolber, J., Albers, M. J., Gram, K. A., Zierhut, M. L.,
961 Park, I., Zhang, V., Hu, S., Nelson, S. J., Vigneron, D. B., Kurhanewicz, J., Dirven, H. A. A. M., and Hurd, R.
962 E.: Imaging Considerations for In Vivo C-13 Metabolic Mapping Using Hyperpolarized C-13-Pyruvate, *Magn.*
963 *Reson. Med.*, 62, 1-10, 10.1002/mrm.21987, 2009.
- 964 Zewe, V., and Fromm, H. J.: Kinetic Studies of Rabbit Muscle Lactate Dehydrogenase, *J. Biol. Chem.*, 237,
965 1668-1675, doi.org/10.1016/S0021-9258(19)83760-2, 1962.
- 966 Zierhut, M. L., Yen, Y. F., Chen, A. P., Bok, R., Albers, M. J., Zhang, V., Tropp, J., Park, I., Vigneron, D. B.,
967 Kurhanewicz, J., Hurd, R. E., and Nelson, S. J.: Kinetic modeling of hyperpolarized C-13(1)-pyruvate
968 metabolism in normal rats and TRAMP mice, *J. Magn. Reson.*, 202, 85-92, 10.1016/j.jmr.2009.10.003, 2010.
- 969